Åbo Akademi University

Neeraj Prabhakar

Multimodal imaging probes and delivery systems for cancer nanomedicine

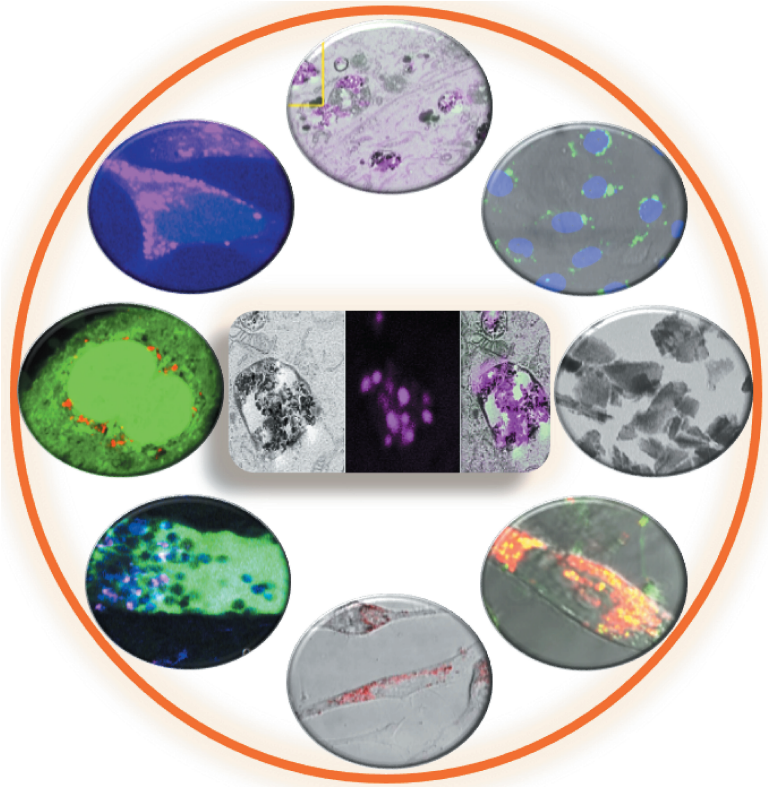

Multimodal imaging probes and delivery systems for cancer nanomedicine

Neeraj Prabhakar

Pharmaceutical Sciences Laboratory
Faculty of Science and Engineering
Åbo Akademi University
Åbo, Finland, 2018

Supervised by

Professor Jessica M. Rosenholm
Pharmaceutical Sciences Laboratory
Faculty of Science and Engineering
Åbo Akademi University, Finland

Co-supervised by

Professor Pekka E. Hänninen
Laboratory of Biophysics
Faculty of Medicine
University of Turku, Finland

Pre-examined by

Professor Niko Hildebrandt
Institute for Integrative Biology for the Cell
Universite Paris-Saclay, France

and

Associate Professor Clare J.Strachan
Division of Phramaceutical Chemistry and Technology
University of Helsinki, Finland

Opponent

Professor Matthias Nees
Pharmaceutical Management and Technology
SRH Fernhochschule, Germany

ISBN 978-952-12-3674-7 (Print)
ISBN 978-952-12-3675-4 (PDF)
Painosalama Oy- Turku, Finland (2018)

"*There is a lot of hard work that needs to be done*"

Martti Ahtisaari

Abstract

Nanoparticles have emerged as one of the most promising tools for addressing central challenges in cancer diagnostics and therapy. This thesis presents the design, surface functionalization, biocompatibility, intracellular interactions and applicability of nanoparticles as potential tools for cancer diagnosis and RNAi therapeutics. The thesis is divided into two parts; 1) cancer cell imaging and 2) siRNA delivery.

In part 1, studies were performed with inherently fluorescent carbon-based nanoparticles (nanodiamonds, NDs, and nanographene oxide, nGO) in order to evaluate their suitability for cancer cell imaging (*in vivo* and *in vitro*). A novel application of NDs in super resolution correlative light and electron microscopy is presented here, whereby NDs are used as a dual-purpose fluorescent and electron dense probes for correlative multi-modal microscopy. Further, the intracellular interactions of NDs are studied to understand the biocompatibility of non-degradable NDs and the reasons underlying the biocompatibility.

Moreover, this thesis elucidates the role of organic surface modifications for enhancing the optical properties of nanographene oxide (nGO) for *in vivo* imaging. When nGO was surface functionalized with the organic polymer PEG-PEI (polyethyleneimine – a polyethylene glycol co-polymer), and attached to the cancer cell affinity ligand FA (folic acid), its dispersibility, cellular internalization and quantum efficiency were improved compared to the non-modified nGO. The surface functionalized nGOs were further applied as optical markers for the non-invasive *in vivo* imaging of cancer cells in a model organism. The nGOs were found to be well suited for detecting cancer cells over the studied 1-week period.

In part 2, systems for the efficient delivery of therapeutic cargo to cancer cells were studied using a nanodiamond (ND) - silica (MSN) composite (ND@MSN) and mesoporous silica nanoparticles (MSN) with redox responsive linkers. ND@MSN, a novel composite material was synthesized by taking advantage of the properties of both the ND (photoluminescence) and the MSN (drug-delivery). The validation of ND@MSN for drug delivery was performed by surface functionalizing the composite particles with the co-polymer PEG-PEI and by loading the ND@MSN with a hydrophobic luminescent dye, which acted as a model drug. The intracellular

delivery of a hydrophobic drugs is generally challenging, but the ND@MSN surface functionalized with co-polymers (Cop) demonstrated excellent efficiency for the intracellular delivery of the hydrophobic model drug. Other noteworthy features related to the use of ND@MSN-Cop were that no premature extracellular release of the dye was observed, that the endosomal escape and intracellular release of the cargo were achieved and that the subsequent tracking of the NDs in the cell was possible.

For the delivery of siRNAs into cancer cells, the MSN nanocarriers were synthesized, in attempt to overcome challenges associated with the *in vivo* delivery of siRNA. Hyperbranched PEI and redox-responsive intracellular triggerable bonds were thus incorporated into the developed MSN nanocarriers. The design of the MSN nanocarriers took into consideration important aspects of *in vivo* delivery, such as the high loading of siRNA, intracellular cleavable linkers, high cellular uptake, and a large pore size to host the siRNA molecules and to protect them from degradation. In the experimental set-up, the MSN nanocarriers demonstrated the sustained intracellular release of the siRNA (120h), while offering protection from enzymatic degradation. The gene knockdown efficiency was further evaluated using a transfection control siRNA. The MSN nanocarriers performed remarkably well and showed excellent transfection efficiency.

Sammanfattning

Nanopartiklar utgör lovande verktyg för att ta itu med centrala utmaningar inom cancerdiagnostik och terapi. Denna avhandling presenterar design, ytfunktionalisering, biokompatibilitet, intracellulära växelverkningar och tillämplighet av nanopartiklar som potentiella verktyg för cancerdiagnos och RNAi-terapi. Avhandlingen är uppdelad i två delar: 1) cancercellsavbildning och 2) tillförsel av siRNA.

I del 1 genomfördes studier med naturligt fluorescerande kolbaserade nanopartiklar (nanodiamanter, ND och nanografenoxid, nGO) för att utvärdera deras lämplighet för cancercellsavbildning (*in vivo* och *in vitro*). En ny tillämpning av ND i superupplöst, korrelativ ljus- och elektronmikroskopi presenteras här, varigenom ND används som ett fluorescerande och elektron-tätt avbidningsmedel med dubbelfunktion för korrelativ multimodal mikroskopi. Vidare studeras de intracellulära växelverkningarna hos ND för att förstå biokompatibiliteten hos dessa icke-nedbrytbara ND och orsakerna bakom den observerade biokompatibiliteten.

Vidare belyser denna avhandling rollen hos organiska ytmodifieringar för att förbättra de optiska egenskaperna hos nanografenoxid (nGO) för *in vivo* avbildning. När nGO ytfunktionaliserades med den organiska polymeren PEG-PEI (polyetylenimin-polyetylenglykol sampolymer) vilken var vidare kopplad till cancercellaffinitetsliganden FA (folsyra), förbättrades dess dispergerbarhet, cellupptag och optiska egenskaper jämfört med icke-modifierad nGO. De ytfunktionaliserade nGO partiklarna användes vidare som optiska markörer för icke-invasiv *in vivo* avbildning av cancerceller i en modellorganism. nGO partiklarna befanns vara väl lämpade för att detektera cancerceller under den studerade perioden på en vecka.

I del 2 studerades läkemedelsadministrationssystem för effektiv transport av terapeutiska molekyler till cancerceller genom användning av ett nanodiamant (ND) -kiseldioxid (MSN) -kompositmaterial (ND@MSN) och mesoporösa kiseldioxid nanopartiklar (MSN) med redox-responsiva länkare. Det nya ND@MSN kompositmaterialet syntetiserades för att utnyttja egenskaperna hos både ND (fotoluminescens) och MSN (läkemedelstillförsel). Utvärderingen av ND@MSN för läkemedelsadministration utfördes genom ytfunktionalisering av partiklarna med

den ovan nämnda sampolymeren (PEG-PEI) och genom att ND@MSN partiklarna laddades med ett hydrofobt luminescerande färgämne, vilket fungerade som ett modellläkemedel. Den intracellulära tillförseln av ett hydrofobt läkemedel är i allmänhet utmanande, men ND@MSN-partikelytan funktionaliserad med sampolymer (Cop) uppvisade utmärkt effektivitet för intracellulär tillförsel av det hydrofoba modellläkemedlet. Andra anmärkningsvärda egenskaper relaterade till användningen av ND@MSN-Cop var att ingen prematur extracellulär frisättning av färgämnet observerades, intracellulär frisättning av de aktiva molekylerna uppnåddes och att den efterföljande spårningen av ND i cellen var möjlig.

För tillförsel av siRNA till cancerceller syntetiserades MSN bärarpartiklar i försök att övervinna de utmaningar som är förknippade med *in vivo* administrering av siRNA. Hyperförgrenad PEI och redox-responsiva intracellulärt klyvbara bindningar införlivades således i dessa nyutvecklade MSN bärarpartiklarna. Utformningen av MSN bärarpartiklar tog hänsyn till viktiga aspekter för *in vivo* administrering, såsom hög laddningsgrad av siRNA, intracellulärt klyvbara länkare, högt cellupptag och en stor porstorlek som kan inhysa siRNA-molekylerna samt skydda dem mot nedbrytning. I den experimentella uppställningen demonstrerade MSN bärarpartiklarna fördröjd intracellulär frisättning av siRNA (120h) samtidigt som skydd mot enzymatisk nedbrytning tillhandahölls. MSN bärarpartiklarna fungerade anmärkningsvärt bra och uppvisade utmärkt transfektionseffektivitet.

List of original publications

I. Core–shell designs of photoluminescent nanodiamonds with porous silica coatings for bioimaging and drug delivery II: application

Neeraj Prabhakar, Tuomas Näreoja, Eva von Haartman, Didem Şen Karaman, Hua Jiang, Sami Koho, Tatiana A Dolenko, Pekka E Hänninen, Denis I Vlasov, Victor G Ralchenko, Satoru Hosomi, Igor I Vlasov, Cecilia Sahlgren, Jessica M Rosenholm, *Nanoscale* 5, **2013**, 3713–3722.

II. Intracellular trafficking of fluorescent nanodiamonds and regulation of their cellular toxicity

Neeraj Prabhakar, Meraj. H. Khan, Markus Peurla, Huan-Cheng Chang, Pekka .E. Hänninen, Jessica. M. Rosenholm, *ACS Omega* 2**, 2017,** 2689–2693.

III. STED-TEM correlative microscopy leaveraging nanodiamonds as intracellular dual-contrast markers

Neeraj Prabhakar, Markus Peurla, Sami Koho , Takahiro Deguchi, Tuomas Näreoja, Huan-Cheng Chang, Jessica M. Rosenholm, Pekka. E. Hänninen. *Small,* **2017**, 1701807.

IV. Functionalization of graphene oxide nanostructures improves photoluminescence and facilitates their use as optical probes in preclinical imaging

Neeraj Prabhakar, Tuomas Näreoja, Eva von Haartman, Didem Şen Karaman, Sergey A Burikov, Tatiana A Dolenko, Takahiro Deguchi, Veronika Mamaeva, Pekka E Hänninen, Igor I Vlasov, Olga A Shenderova, Jessica M Rosenholm, *Nanoscale*, 7, **2015**, 10410-10420.

V. Stimuli-responsive hybrid nanocarriers developed by controllable integration of hyperbranched PEI with mesoporous silica nanoparticles for sustained intracellular siRNA delivery

Neeraj Prabhakar, Jixi Zhang, Diti Desai, Eudald Casals, Tina Gulin-Sarfraz, Tuomas Näreoja, Jukka Westermarck, Jessica. M. Rosenholm, *International Journal of Nanomedicine, 11,* **2016**, 6591–6608.

VI. Design considerations for mesoporous silica nanoparticulate systems in facilitating biomedical applications

Diti Desai, Didem Sen Karaman, **Neeraj Prabhakar**, Sina Tadayon, Alain Duchanoy, Diana M. Toivola, Sadhana Rajput, Tuomas Näreoja, Jessica M. Rosenholm, *Mesoporous Biomater.* 1, **2014**.

Contribution of the author

In PAPER I, the author was responsible for the biological evaluation of the nanodiamond-silica composites. The author contributed to the writing of the first draft. Tuomas Näreoja performed the STED imaging and contributed to writing the manuscript. Eva von Haartman synthesized the nanodiamond-silica composites.

In PAPER II, the author performed *in vitro* experiments and analysed the intracellular trafficking mechanism of the nanodiamonds. The author wrote the first draft. Meraj Khan performed western blotting. Markus Peurla performed the transmission electron microscopy analysis of nanodiamond localization in cells.

In PAPER III, the author performed and developed a method for correlative microscopy. Markus Peurla performed transmission electron microscopy with the cells. Sami Koho performed software based image correlation. The author wrote the first draft of the manuscript.

In PAPER IV, the author performed an *in vitro* and *in vivo* imaging established CAM model for *in vivo* studies. The author wrote the first draft of the manuscript. Tuomas Näreoja contributed to *in vivo* imaging and manuscript writing. Eva von Haartman performed material characterization. Didem Sen Karaman performed the surface functionalization of the nanographene oxides.

In PAPER V, the author performed the *in vitro* evaluation of the MSN nanocarriers for RNAi therapy. The author wrote the first draft of the manuscript. Jixi Zhang synthesized the MSN nanocarriers and performed the material characterization. Diti Desai performed the loading of the siRNA.

In PAPER VI, the author performed two-photon *in vivo* imaging and the lifetime measurement of the fluorescence.

Abbreviations

AFM	Atomic force microscopy
APD	Avalanche photodiode
CAM	Chorioallantoic membrane
CLEM	Correlative light electron microscopy
C-dots	Carbon dots
Composite	Nanodiamond silica composite
Cop	PEG-PEI copolymer
DAPI	4',6-Diamidino-2-Phenylindole, Dihydrochloride
DiI	1,1'-Dioctadecyl-3,3,3',3'-Tetramethylindocarbocyanine Perchlorate
EPR	Enhanced permeability and retention
FA	Folic acid
FCS	Fetal calf serum
FITC	Fluorescein isothiocyanate
FR	Folate receptor
GFP	Green fluorescent protein
HRTEM	High-resolution transmission electron microscopy
HyD	Hybrid detector
LAS	Leica application Suite
MSN	Mesoporous silica nanoparticles
MP	Multi-photon

MRI	Magnetic resonance imaging
NA	Numerical aperture
ND	Nanodiamond
ND@MSN	ND-MSN composite
nGO	Nanographene oxide
NP	Nanoparticle
NV	Nitrogen Vacancy
PEG	Polyethylene glycol
PEI	Polyethylenimine
PFA	Paraformaldehye
PL	Photoluminescence
QD	Quantum dots
RFP	Red fluorescent protein
RISC	RNA induced silencing complex
SN	Silica nanoparticle
siRNA	Small interfering RNA
STED	Stimulated emission depletion
TEM	Transmission electron microscopy
YFP	Yellow fluorescent protein

List of supporting publications

i. **Gold nanoparticle printed coverslips to facilitate fluorescence-TEM correlative microscopy**
Neeraj Prabhakar, Anni Määttänen, Jouko Peltonen, Pekka Hänninen, Markus Peurla, Jessica M Rosenholm. *Microscopy*, **2017**, 1-4.

ii. **Targeted modulation of cell differentiation in distinct regions of the gastrointestinal tract via oral administration of differently PEG-PEI functionalized mesoporous silica nanoparticles**
Diti Desai, **Neeraj Prabhakar**, Veronika Mamaeva, Didem Şen Karaman, Iris Lähdeniemi, Cecilia Sahlgren, Jessica .M Rosenholm, Diana. M Toivola. *International Journal of Nanomedicine,* 11, ***2016,*** 299–313.

iii. **Semiconducting Polymer Encapsulated Mesoporous Silica Particles with Conjugated Europium Complexes: Toward Enhanced Luminescence under Aqueous Conditions**
Jixi Zhang, **Neeraj Prabhakar**, Tuomas Näreoja, Jessica. M Rosenholm. *ACS Applied Material and Interfaces,* 6 (21), **2014**, 19064–19074.

iv. **Microwave-assisted one-step synthesis of acetate-capped $NaYF_4$:Yb/Er upconversion nanocrystals and their application in bioimaging**
Kumbam Lingeshwar Reddy, **Neeraj Prabhakar**, Riikka Arppe, Jessica M. Rosenholm, Venkata Krishnan. *Journal of Material Sciences,* **2017**, *52* (10).

v. **On the intracellular release mechanism of hydrophobic cargo and its relation to the biodegradation behavior of mesoporous silica nanocarriers**
Eva von Haartman, Desiré Lindberg, **Neeraj Prabhakar**, Jessica. M. Rosenholm. *European journal of pharmaceutical sciences,* **2016**, *95*, 17–27.

vi. **Controlled synthesis, bioimaging and toxicity assessments in strong red emitting Mn^{2+} doped $NaYF_4$:Yb^{3+}/Ho^{3+} nanophosphors**
Kumbam Lingeshwar Reddy, Monika Rai, **Neeraj Prabhakar**, Riikka Arppe, S. B. Rai, Sunil Kumar Singh, Jessica M. Rosenholm, Venkata Krishnan. *RSC Advances*, **2016**, *6* (59).

vii. **Prolonged Dye Release from Mesoporous Silica-Based Imaging Probes Facilitates Long-Term Optical Tracking of Cell Populations In Vivo**
Jessica M. Rosenholm, Tina Gulin-Sarfraz, Veronika Mamaeva, Rasmus Niemi, Ezgi Özliseli, Diti Desai, Daniel Antfolk, Eva von Haartman, Desiré Lindberg, **Neeraj Prabhakar**, Tuomas Näreoja, Cecilia Sahlgren. *Small,* **2016**, *12* (12).

viii. **Ratiometric Sensing and Imaging of Intracellular pH Using Polyethylenimine-Coated Photon Upconversion Nanoprobes**
Tuomas Näreoja, Takahiro Deguchi, Simon Christ, Riikka Peltomaa, **Neeraj Prabhakar,** Elnaz Fazeli, Niina Perälä, Jessica M Rosenholm, Riikka Arppe, Tero Soukka, Michael Schaeferling. *Analytical Chemistry.* **2017**, *89* (3), 1501–1508.

Contents

1 Introduction

Nanotechnology is an interdisciplinary field that includes the synthesis, design, and application of nanomaterials[1]. In the last several decades, biomedical nanotechnology has focused primarily on the development of drug-delivery systems and diagnostic probes[2–5]. The most notable examples of nanotechnology in cancer research include the targeted delivery of anti-cancer drugs[6–8], nanosized contrast agents for magnetic resonance imaging[9–11], liposomes for breast cancer therapeutics[12–14], and the highly specific detection of DNA and proteins[15,16]. Nanotechnology is recognized as one of the leading technologies for making significant advances in cancer theranostics (diagnostics and therapy)[2,3]. The physiochemical properties of nanomaterials significantly differ from the bulk materials. Nanotechnology allows tuning the shape, size, and surface properties of nanomaterials for the loading of therapeutic or imaging agents with high stability, while maintaining compatibility with biological fluids[17]. The nanoscale-sized nanomaterials allow a larger surface area for loading of the therapeutic agents as well as interactions with biomolecules at the same scale. For example, mesoporous silica nanoparticles (MSNs) are porous, surface modifiable, biodegradable materials, which offer a large surface to volume ratio[18–20]. The large surface area can be used to load therapeutic agents via non-covalent physical adsorption or by covalent bonding.

Applications of nanotechnology in cancer treatment have the potential for the selective administration of therapeutic molecules to target organs with minimal side effects. Nanotherapeutics are growing at a steady rate in clinical and research applications[21,22]. A few commercially approved nanopharmaceuticals for the treatment cancer already exist. Notable commercially available nanopharmaceutical products include Doxil®, Myocet®, Eligard®, and Opaxio® [23]. The translation of results obtained from biomedical research into clinical applications and successful commercial products is a long and risky path. However, there is considerable optimism that nanoparticles would provide a theranostics approach for treating cancer.

Molecular heterogeneity[24,25] and drug resistance[26–28] present daunting challenges for the treatment of cancer. Cancerous cells show a molecular heterogeneity between the primary and metastatic tumors[29–32] as well as resistance towards chemotherapy[26,28]. The multitude of heterogeneity among cancer phenotypes can allow a sub-

population of cancerous cells to circumvent monotherapy[31]. New targeted therapies, based on personalized medicine can offer an approach to treating cancer in a way that takes into account the genetic profiles of tumors in individual patients[33,34]. Since traditional chemotherapeutic treatments might respond differently to the individual genetic makeup of patients, these new approaches are expected to provide solutions for the complex challenges in cancer treatment

One of the latest approaches for treating cancer is based on the therapeutic delivery of a siRNA (small interfering RNA)[35]. siRNAs are 21-25 nucleotides long, naturally evolved molecules with roles in essential cellular responses[36]. A siRNA causes the selective silencing and degradation of a target mRNA[37]. A siRNA based approach could allow the specific degradation of oncogene mRNAs, which are involved in the molecular pathways that drive cells into malignancy. Recent therapeutic applications have demonstrated the potential of using siRNAs for treating different types of cancers such as HER2-positive breast cancer[38]. RNAi (RNA interference) has the potential to overcome present challenges that cancer treatment faces, such as drug resistance[38,39]. siRNA therapy has shown the potential for overcoming drug resistance in a study with the breast cancer drug, trastuzumab[38]. However, the applications of siRNA in cancer therapy have been restricted mainly to *in vitro* studies, due to the unavailability of efficient platforms for *in vivo* delivery[40,41]. RNAi therapeutics requires *in vivo* delivery vehicles that provide high bioavailability, a high loading degree, targeted delivery to tumors and protection of the siRNAs for sustained targeted release[42,43]. NPs could be ideal delivery vehicles for siRNA for applications in *in vivo* tumor targeting. NPs based platforms offer the potential for overcoming challenges posed by the current *in vivo* delivery vehicles[42,44–46]. NPs have several characteristics that qualify them as one of the preferred siRNA delivery vehicles for *in vivo* cancer therapeutics. The characteristics and their significance for siRNA delivery systems are discussed in the following chapters.

Nanomedicine could provide an integrated platform for diagnosing, targeting drug-delivery and monitoring the therapeutic response in cancer treatment. Combining diagnostic imaging with therapy could enable the development of responses to challenges posed by cancer treatment. Multimodal, non-invasive, high-resolution imaging is emerging as a powerful tool for providing cellular/molecular information for applications in cancer diagnostics[47–51]. The targeted delivery of imaging agents can be achieved by the conjugation of molecules that recognize specific cell surface

markers [52–54]. The targeted delivery of contrast agents can be used for whole tumor mapping. Nanoparticles can be used as contrast agents with fluorescence microscopy[55–58] and magnetic resonance imaging (MRI)[9,11]. Inherently fluorescent or fluorophore conjugated nanoparticles are currently being studied for applications in different bioimaging techniques. Bioimaging with fluorescent nanoparticles can be used in three different techniques. 1) microscopic detection of cells with internalized fluorescent nanoparticles[59,60]; 2) targeted bioimaging of specific cells or cellular structures using antibodies, ligands or oligomers attached to nanoparticles for specific recognition[52,54]; 3) nanoparticles can be used as chemical sensors for imaging disease-related changes in the distribution of chemical species such as pH, calcium, oxygen etc[61].

2 Review of the Literature

2.1 Optical probes for cell imaging

Fluorescence microscopy is rapidly evolving with the technical improvements to imaging instruments, imaging probes and imaging methods[62–68]. Over the years, the technological advancements have focused on the development of improved contrast agents, new kinds of instruments, and higher resolution imaging[64].

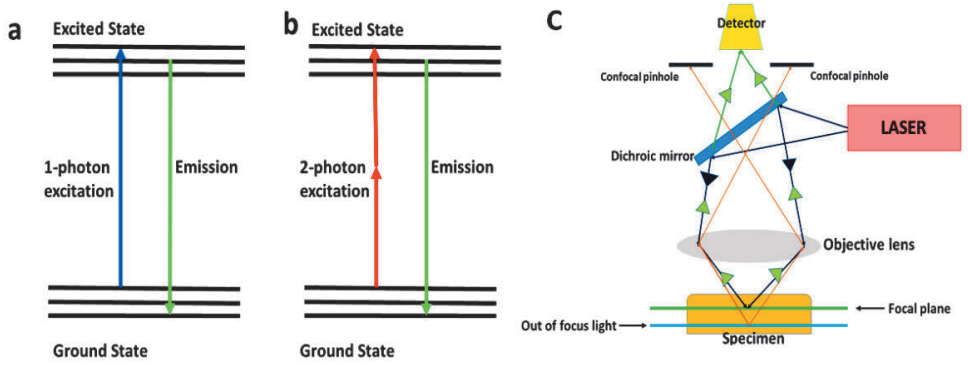

Figure 1. Schematic representation of the principle of fluorescence emission and confocal microscopy. a) Fluorophores can be excited with a single photon of a suitable shorter wavelength. The fluorophore absorbs the energy and enters the excited state. In the excited state, the fluorophore releases energy in the form of heat and vibration. It relaxes to the ground state by emitting a longer wavelength. b) Fluorophores can be excited by the process of two-photon excitation, where two photons of a longer wavelength are used to provide sufficient energy for excitation and the fluorophore emits a shorter wavelength. c) The principle of confocal microscopy is based on the application of confocal pinholes that selectively collect the in-focus light from the specimen's focal plane and point by point illumination of the sample.

One of the most commonly used fluorescence-based cell imaging techniques is confocal microscopy. Confocal microscopy is a laser scanning based microscopy method that is compatible with fixed and live cell imaging. Confocal microscopy is based on two principal ideas: 1) rejection of out of focus light by utilizing confocal pinholes and 2) point by point specimen illumination[69]. The optical resolution offered by a confocal microscope is limited by the diffraction of light and its spatial resolution, approximately 250-300nm.

Two-photon microscopy is a commonly used fluorescence microscopy technique, based on nonlinear interactions between light and a fluorophore[70–72]. The fluorescence generated by a two-photon process depends on the absorption of two photons simultaneously by the same molecule. These photons have longer wavelengths, mostly infra-red wavelengths, each of these photons carries one-half of the excitation energy[71]. Since the wavelength and the energy of photons are inversely proportional, the wavelength of these two photons is theoretically 2X times longer than the single-photon excitation wavelength. The major application of using two-photon excitation microscopy is for *in vivo* imaging[72]. Using a longer excitation wavelength allows deeper penetration into animal or thick tissues compared to single-photon microscopy. Two-photon excitation microscopy has other advantages such as less photobleaching, low auto-fluorescence, no requirement of pinholes for the collection of in-focus light compared to single photon microscopy[73].

In last decade, the development of super resolution fluorescence microscopes has circumvented the resolution limit of light by utilizing novel methods such as STED (Stimulated emission depletion) [74–76], SIM (Structure-illuminated microscopy)[77,78], PALM (Photoactivated localization microscopy)[79,80] and other similar super resolution techniques[81]. Among them, STED was the first super resolution technique to break the barrier of the diffraction limit of light and it was based on the de-excitation of fluorophores using stimulated emission depletion[75]. STED techniques have been demonstrated for the imaging of fixed as well as live cells[82–85]. STED techniques could achieve a superior resolution (X-Y) up to 6-30nm[76,83]. The advancement in resolving nanoscale objects with fluorescent microscopes has played a vital role in the understanding of the precise localization of molecules within cells.

Fluorescence imaging requires fluorophores for microscopic visualization. Thousands of organic fluorophores have been devised to provide labels for biological systems. The large spectral range of organic fluorophores can be applied at the cellular and sub-cellular level and specific labeling at the molecular level. The development of intrinsic fluorescent proteins has allowed biologist to genetically tag a protein of interest in living organisms or individual cells[86]. The most commonly used fluorescent proteins belong to the green fluorescent protein (GFP) family. There are multiple derivatives of GFP, such as red fluorescent proteins (RFP), yellow fluorescent protein (YFP), which offer a wide selection in the visible range (400-700 nm). The desirable characteristics of fluorophores include 1) a specific excitation

wavelength; 2) detectability with fluorescence microscopy; 3) a high molar absorption coefficient, bright with a high quantum yield; 4) solubility in relevant cell media; 5) photostablity[87] and 6) properties that allow it to be used as a tag or mean that it can be genetically expressed within the target cells, or both.

Organic fluorophores and fluorescent proteins are compatible with advanced imaging techniques such as laser scanning confocal microscopy, two-photon microscopy[88] and superresolution fluorescence techniques[89,90]. Practically, a fluorophore can be recycled from the ground state to the excited state infinite times, but fades by a phenomenon known as photobleaching[87]. The bleaching of the fluorophore is a generic term for all associated processes that contribute to the loss of the fluorescent signal. In case of organic fluorophores and fluorescent proteins, bleaching can occur at the molecular level in several different ways[87]. In general, bleaching of the fluorophore is mainly associated with triplet states. Long-lived triplet states of fluorophores have a higher probability of interacting with molecular oxygen. Singlet oxygen or any reductive species can interact with fluorophores and covalently alter the activity of the fluorophores[91]. The process of bleaching is a major problem with organic fluorophores and fluorescent proteins.

2.2 Nanoparticles as bioimaging probes

To overcome current existing shortcomings associated with fluorophores, NPs could be a powerful tool for labeling cells in disease diagnostics[49,92–94]. NPs offer advantages over traditional fluorophores for targeted imaging[57,95,96]. NPs can be tuned with proper surface functionalization to attach specific molecules for the targeted imaging of cancer cells, with the added advantage of being fluorescently detectable. Targeted bioimaging can be performed with the attachment of cancer cell targeting ligands[97,98], oligomers[99], or antibodies to the surface of the nanoparticle [52]. Typically, NPs conjugated or labeled with an organic fluorophore, as well as inherently fluorescent NPs have shown to be virtually inert, with little interaction with cellular proteins[100]. Moreover, they have generally demonstrated distinctly better photostability in comparison to their free-dye counterparts[101,102].

Multiple types of NPs are used for bioimaging, including nanoparticles derived from silica[19,103], quantum dots[57], gold nanoparticles[104], fluorescent carbon nanoparticles[105], upconversion nanomaterials[106,107], and lanthanide materials[108,109]. C-dots (carbon

dots), a carbon based imaging nanoprobe, has entered human trials for its potential applications[110]. Silica-based nanoparticles (SNs) were the first nanoparticle to be applied for bioimaging applications[100]. SNs are inherently non-fluorescent, however, imaging agents can be incorporated into them by either physical adsorption or chemical conjugation. MSNs have been used in cell imaging and molecular sensing[111]. Silica nanoparticles (SNs) are most commonly used due to their high loading capacity of fluorescent dyes [100]. SNs can be surface conjugated with lanthanide luminescent chelates such as europium, terbium, and gadolinium[112–114]. SNs have shown low cytotoxicity and efficient cell imaging capabilities[115].

Inherently fluorescent NPs also exist. These include quantum dots, carbon dots, nanodiamonds, single and multi-walled carbon nanotubes,[55,57,116–118] upconverting NPs[106] and lanthanide doped NPs[114]. Fluorescent NPs have in general shown good contrast and good photostability, and their sizes are on the nanometer scale, which facilitates their internalization into cells[100]. These NPs have shown different degrees of toxicity toward cells. One popular example is the application of quantum dots (QDs) for cell imaging. QDs exhibit high photostability and size dependent emission over the entire visible wavelength[57]. QDs can be readily internalized by the cells, however, their clearance from tissues can be challenging. Moreover, QDs have shown to interact with the thiol groups of cysteine in the cellular proteins and can exhibit toxic effects due to the leakage of heavy metals in cells[100].

Table 1. List of commonly used inherently fluorescent nanomaterials for bioimaging.

Nanomaterial	Material source
Quantum Dots	Semiconductor metals (Zn, Cd, Se)
Carbon Dots	Carbon
Nanodiamonds	Carbon
Nanographene Oxide	Carbon
UCNPs	NaYF4 (Doped with Er(III), Yb(III) or Tm(III))

Among the fluorescent nanoparticles, carbon based inherently fluorescent NPs can be used as promising substitutes for overcoming the toxic effects of semiconductor quantum dots[119,120]. Fluorescent carbon nanoparticles such as nanodiamonds (NDs), carbon dots, nanographene oxide (nGO), fullerenes, and carbon nanotubes are being explored for their potential applications in bioimaging due to their unique optical

nature and high biocompatibility[121] -the major component of these materials being carbon, a non-toxic "element of life".

Fluorescent carbon nanomaterials can be synthesized by different methods. For an example, NDs can be synthesized by detonation based methods on a commercial scale[117]. Another such example of chemical synthesis is the synthesis of nanographene oxide by the oxidation of micro or nanographite by a 3:1 ratio of a mixture of sulfuric to nitric acid [122].

NDs and nGOs have shown to be non-toxic and stable optical markers for bioimaging[60,123]. They possess unique optical properties well suited for bioimaging applications. In case of NDs, the fluorescence originates from defects in the crystal lattice of diamonds. NDs have more than 500 optical centers. Among them, negatively charged nitrogen vacancies (NV^-) are the most studied due to their photostability[65,124,125].

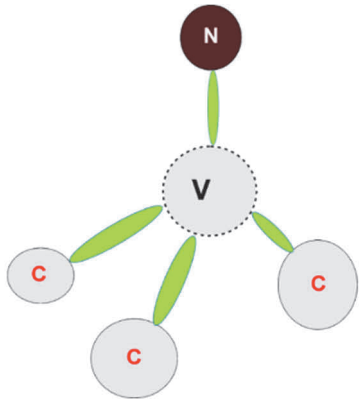

Figure 2. Schematic representation of a photostable nitrogen-vacancy center. In the diamond lattice, a nitrogen atom (N) is substituted by carbon (C), adjacent to a vacant space (V)[126].

NDs can be typically excited at 480- 532 nm and the emission wavelength of NDs lies in the red range (650-800 nm)[55,60,76]. The emission in the red range is well-suited for deep tissue imaging. NDs are well-suited for different multi-modal microscopy applications such as live cell imaging, super resolution STED imaging[76] and multi-photon microscopy. Additionally, the electron dense nature of NDs can be used for visualization with electron microscopy[60]. The unique optical and electron dense properties of NDs are well-suited for further applications through method

development for correlative microscopy, where there is a growing need for unique landmarks that can be detected with both optical and electron microscopes[127,128].

Nanographene oxide (nGO) also belongs to the family of fluorescent carbon nanomaterials [95,122,123]. They have unique optical properties comparative to those exhibited by the QDs. nGOs have demonstrated excitation dependent emissions, which can be detected throughout the visible spectrum. nGO nanoparticles have generally shown to be biocompatible with cells[120] and they have demonstrated only weak interactions with cellular proteins[129]. nGOs have been applied to cell, tissue, and small animal imaging[130] and one reported paper suggested that they can efficiently internalize and are mainly localized within the cytoplasmic space[131]. NDs and nGOs can be surface functionalized with organic polymers for enhanced cellular uptake, better colloidal stability, prevention of aggregation and could influence their optical properties[60,123].

2.3 Surface functionalization of nanoparticles

Surface functionalization of NPs is a commonly used strategy for reducing interactions with the immune system[115,132,133]. Surface functionalization of NPs influences their cellular internalization, intracellular delivery, specific cell recognition, nanoparticle stability and endosomal escape of cargo[133–136]. The basic design of surface functionalization can be varied according to the nature of the application. In case of cancer nanomedicine, the general strategy used for surface functionalization includes the attachment of affinity ligands[98,137] or antibodies[53] for the recognition of cancer cells, polymeric coating for enhanced cellular uptake[115,134,138,139] or the endosomal escape of a drug or siRNA[140,141], and the conjugation or surface doping of imaging agents[60,114].

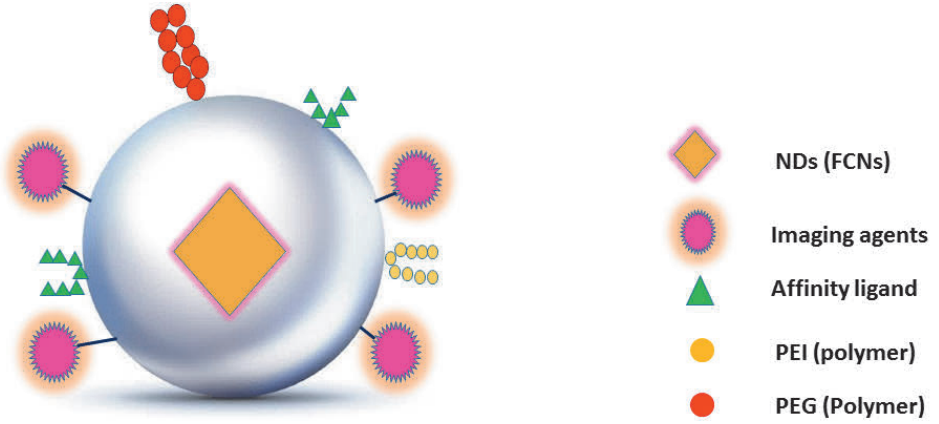

Figure 3. Schematic depiction of nanoparticle surface modifications for applications in cancer nanomedicine. Nanoparticles can be surface functionalized with the PEI-PEG polymer (positively charged + colloidally stable). Attachment of cell surface recognizing peptides, antibodies, ligands etc. Imaging agents can be either chemically conjugated or physically adsorbed.

NPs have been surface functionalized with a wide variety of surface recognition molecules (peptides[142,143], antibodies[144], or ligands[145–147]). The attachment of surface recognition molecules (active targeting) improves the differential affinity toward specific proteins being present on the cell surface. Commonly used receptors for cancer cell targeting include folate receptors[148,149], transferrin receptors[150,151], and lectin receptors[152,153] etc. For example, folate receptors (FR) are overexpressed in a majority of cancer cells[97,148]. Cancers known to overexpress folate receptors include breast, lung, kidney, ovarian and brain tumors. The surface functionalization of NPs with folic acid (the ligand for FR) may thus enhance their specific cellular uptake into tumor cells.

The targeted cellular uptake of ligand attached NPs (active targeting[154,155]) can be further enhanced by surface coating the NPs with polymers (passive targeting[156]). Surface functionalization with polymers contributes to the stability of the NPs and enhances passive targeting. NPs have generally demonstrated preferential extravasation into the leaky tumor vasculature as compared to healthy tissues. NPs thereby remain localized due to an enhanced permeability and retention (EPR) effect (passive targeting) [2,157,158]. An example is this is coating NPs with PEG (polyethylene glycol). PEG coating enhances the circulation time of the NPs and prevents the adsorption of blood serum proteins with low toxicity[159–161]. In order to facilitate

cellular uptake, NPs can be coated with a combination of polymers along with PEG[123,134,139]. One such additional coating can be performed with the PEI (polyethyleneimine) polymer. PEIs are synthetic cationic polymers that provide a high positive charge on the NP surface[132,133]. The positive charge on the NP surface influences cellular uptake, endosomal escape[162,163] and enhances the loading of DNA and the delivery of siRNA for the gene therapy of cancer cells[164].

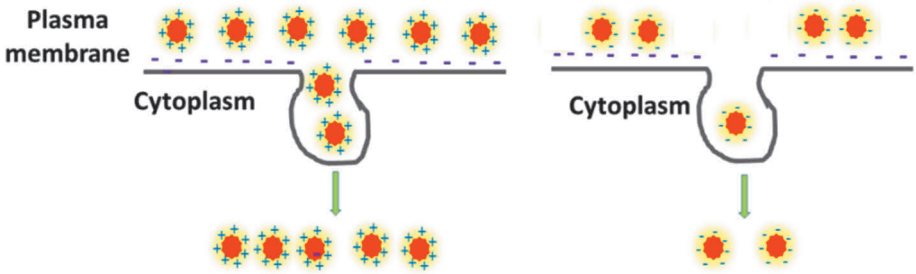

Figure 4. Schematic representation of interactions between NPs bearing positive and negative charges with the negatively charged lipid bilayer. NPs coated with apositively charged functional group (PEI) show high affinity or cell membranes. Instead, the negatively charged NPs have demonstrated a lower affinity for interactions with the cell membrane.

Knowledge about interactions between NPs and the lipid bilayer of the cell membrane is critical when designing applications such as imaging, phototherapy, and gene therapy[132,133,165]. The presence of positively charged groups, such as PEI play a crucial role in NPs interactions with the lipid bilayer of the cell membrane, and can maximize cellular uptake[132,133]. It has been demonstrated that NPs bearing a negative or neutral surface charge are less-well adsorbed on the cell membrane than are positively charged NPs. These non-positively charged NPs shows less cellular internalization in comparison to the NPs with a positive surface charge.

2.4 siRNA nanomedicine therapy for cancer

RNA interference (RNAi) is an evolutionarily conserved mechanism for the regulation of endogenous pathways by selectively inhibiting the expression of mRNA[36,166]. The specific silencing by double-stranded RNAs was first observed by Fire and Mellow in *Caenorhabditis elegans*[37]. Later, the specific mechanism was

described in plant and mammalian cells[40]. The application of synthetic siRNA for mRNA silencing and mechanism of RNAi was described by Elbashir et al,[36,166]. In mammalian cells, siRNAs are synthesized from double-stranded exogenous RNA, processed by the enzymatic activity of a ribonuclease enzyme, Dicer[166]. Dicer belongs to the family of RNAse III enzymes and produces small interfering RNA molecules, with the lengths of 21-25 nucleotides. siRNAs are produced by Dicer enzymes form a RISC (RNA induced silencing complex) with Argonaute (Ago) proteins. At RISC, the guide strand is selected for mRNA recognition, whereas the other strand is degraded[167].

The properties of the RNAi pathway can be exploited for the selective regulation of genes of interest. The RNAi pathway could be a potent way developing future therapeutics for the downregulation of oncogenes involved in cancer. RNAi based cancer therapeutics requires delivery vehicles for the efficient transportation of siRNAs to the target cancer cells. In general, siRNAs are prone to degradation by the enzymatic activity of RNAses[168,169].

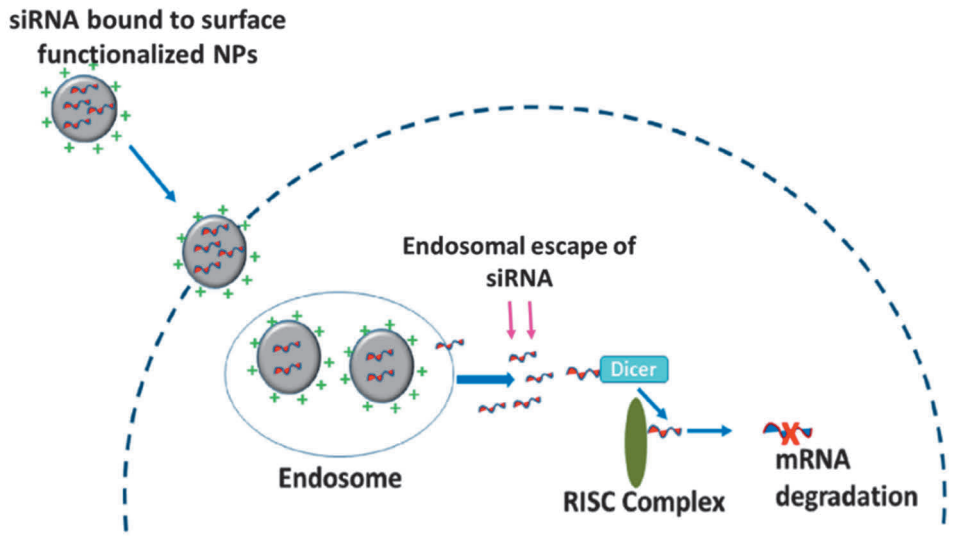

Figure 5. Schematic representation of MSNs as vectors for siRNA delivery. siRNA can be efficiently delivered to cells via organic surface functionalization, and stimuli responsive siRNA release can be achieved by including intracellular redox cleavable linker groups to the MSN.

Despite the presence of numerous vectors for siRNA delivery, most commercial systems have shown efficient delivery only *in vitro*. Moreover, these are not commonly applied for the *in vivo* tumor-targeted delivery of siRNAs. The other concerns with siRNA delivery rise mostly from the nature of the siRNA molecules, such as their low bioavailability, high polarity and poor stability under physiological conditions. Therefore, the design of delivery vehicles should offer consideration to these challenges posed by siRNAs. An efficient *in vivo* system should address issues such as siRNA protection, systematic sustained release, and high loading capacity. Several formulations have been applied to achieve the systemic delivery of siRNAs such as viral vectors[170], polymers[164,171], cationic lipids[172] and inorganic NPs[138,173,174].

Among the above-mentioned approaches, MSN can be utilized for designing a rational delivery system based on the unique characteristics of MSNs[175–177]. They have several characteristics that qualify them as preferred siRNA delivery vehicles for *in vivo* cancer therapeutics. The low cytotoxicity and high cellular uptake of MSNs have been well characterized over the past decade[177–179]. MSNs are synthetically versatile porous materials with an ordered pore structure resulting in a high surface area and large pore volume[180]. These structural characteristics of MSNs can be exploited for reaching a high loading capacity for siRNAs, while the localization of the siRNAs in the pores consequently offers efficient protection from degradation[173,175]. The applicability of MSNs can be tuned for the delivery of siRNAs. For example, modifications in material design would include MSNs with expandable pores for the incorporation siRNAs[175,181]. Stimuli responsive siRNA release from the mesopores of MSNs can be achieved by the inclusion of intracellular redox cleavable linker groups and tethering with hyperbranched poly(ethyleneimine) (PEI)[175]. PEI is a well-recognized organic polymer employed in gene delivery applications[135,163]. PEI has highly positively charged secondary and tertiary amine groups. Under physiological conditions, such as during entrapment in acidic endosomal vesicles, PEI can be protonated in the acidic environment. This leads to the endosomal escape of cargo by the rupture of the endosomes vesicle, which is known as the proton sponge effect[162]. In general, MSNs can be efficiently surface functionalized for the targeted *in vivo* delivery of siRNAs. MSNs can be further conjugated with organic fluorophores to allow their subsequent imaging and detection.

3 Aims of the study

The overall aim of the thesis is to study in detail the multimodal imaging and intracellular trafficking of novel imaging probes and drug/siRNA delivery vehicles.

The specific objectives are:

1. Evaluation of surface functionalized fluorescent probes (NDs and nGO) for cancer cell imaging (Paper I&IV).

2. Investigation of the intracellular trafficking of nanodiamonds and their application as dual probes for correlative light-electron microscopy (Paper II&III).

3. Evaluation of silica coated and surface functionalized NDs as single multi-functional nanoprobes for bioimaging and drug-delivery in cancer cells (Paper I).

4. Development and evaluation of redox responsive MSN nanocarriers for intracellular siRNA delivery into cancer cells (Paper V&VI).

4 Materials and methods

In this section, a short summary of the methods used in the study is given. A detailed description of the phenomena studied and techniques used can be found in the original publications.

Table 2. List of applied techniques for investigating the corresponding phenomena.

Phenomenon studied	Technique used	Publication No
Particle morphology	TEM, AFM	I,IV
Spectral characterization of inherently photoluminescent nanomaterials	Spectrophotometry	I,IV
Cytotoxicity assays	WST-1, Crystal violet staining	I,IV-V
Cellular uptake of nanomaterials	Confocal microscopy	I,IV-V
Cell imaging of nanomaterials	Confocal microscopy	I-II, III-V
Intracellular trafficking of NDs	Confocal microscopy, TEM	II
In vivo imaging of nGO	Two-photon microscopy	IV
In vivo imaging of MSN	Two-photon microscopy	VI
NDs as correlative intracellular probe for STED and TEM	STED, TEM	III
Intracellular drug delivery capacity by ND-SiO_2	Confocal microscopy	I
siRNA delivery by MSN	Live cell microscopy, IncuCyte imaging	V

4.1 Morphology and optical characterization of nanodiamonds and nanographene oxide

Nanoparticle size was studied with TEM (Paper I&IV) and AFM (Paper IV)[60,123]. Photoluminescence (PL) spectra were studied with a spectrophotometer. The PL spectrum of NDs (Paper I) was recorded at 488 nm with a LABRAM HR800 spectrophotometer (HORIBA Instruments, Japan) at room temperature. The PL spectra and quantum yield of nGOs (Paper IV) was recorded with a PTI Quanta-Master spectrofluorimeter (Photon Technology International, USA). The excitation sources were 488 nm (argon laser), diode lasers at 405 nm and 532 nm. The emission was recorded in the range of 410-800 nm.

4.2 Cell Studies

Cell studies were performed with HeLa cells (Paper I), MDA-MB-231 cells (Paper II-V) and A549 cells (Paper IV). Cells were grown in Dulbecco's modified Eagle's medium (DMEM) supplemented with 10% fetal bovine serum, 2mM L-glutamine, and 1% penicillin–streptomycin (v/v). The cells were maintained at 37°C, 5% CO_2.

4.2.1 Cell viability assay

The cell viability assessment of nanomaterials was performed with the WST-1 assay (Paper I, IV-V). WST-1 is a ready-to-use cell viability reagent (Roche Diagnostics, Germany). 10,000 cells per well were added to a 96 well plate containing cell media DMEM and incubated overnight to allow them to adhere to the surface. Cell media containing nanomaterials was added to cells. After, 48-72h, 10 µl of WST-1 was added to each well and left to incubate for 3h at 37°C, 5% CO_2. The absorbance values for each sample were read at 430 nm by Tecan Ultra microplate reader (MTX Lab Systems, Inc.). The observed absorbance value was correlated with the number of viable cells in the presence of positive (toxin) and negative control cells (without nanoparticles).

4.2.2 Cellular uptake and cell imaging

Cellular uptake and cell imaging (fixed cells) measurements were performed with a TCS SP5 confocal microscope (Leica microsystems, Germany). The excitation source was an argon laser at 488 nm for NDs, nGO and MSNs (Paper I-II, IV-V). The emission from nGO, MSNs (FITC) and NDs was collected in the range of 500-550 nm and 650-730 nm. The image acquisition included the LASAF software (Leica application suite), PMT (Photo multiplier tube) and 100X oil objectives (NA 1.45).

4.2.3 *In vivo* imaging (CAM model)

The chick embryo chorioallantoic membrane (CAM) as was used as an *in vivo* animal model for imaging implanted tumors (Paper IV). The CAM model serves as an easy-to-image, fast and inexpensive model for performing short-term *in vivo* experiments[182]. The CAM model was used to image nGO labeled tumors (Paper IV). For cellular applications, nGO nanoparticles were surface coated with PEG (polyethylene glycol) –PEI (polyethyleneimine) polymers (Cop) and the cancer cell affinity ligand, folic acid (FA) was attached to them. The cancer cells (MDA-MB-231, HeLa, and A549) were labeled with nGO-Cop-FA and further, mixed with BD

Matrigel (BD Biosciences, USA) and implanted over the CAM. The tumor was allowed to grow over the CAM for 1 week. The *in vivo* imaging of the nGO labeled tumors was performed with two-photon microscopy[70,73]. The instrumental setup consisted of TCS SP5 MP (Multi-photon, Leica microsystems) with a 20X water dipping objective, Non-descanned detectors (NDD). A Ti-sapphire femtosecond pulse laser at 800 nm was used as the excitation source for nGO-Cop-FA. The emission from nGO-Cop-FA labeled tumors was collected using NDD detectors at 430-480nm.

4.2.4 Intracellular trafficking and investigation of the cellular toxicity of NDs

Intracellular trafficking of NDs was studied with confocal microscopy (2-48h) using early endosomal and lysosomal markers (Paper II). For the intracellular trafficking study, non-functionalized NDs were used to study cellular fate. NDs have been reported to be internalized into a cell by clathrin-mediated endocytosis[119]. EEA1 (early endosomal antigen-1) was used as a specific marker for ND internalization in fixed cells. 1˚anti- EEA1 antibody (ThermoFisher Scientific Inc, USA) was used for marking early endosomes. The localization of NDs and their interactions with lysosomes were studied for 2-48h. LysoTracker Green® (ThermoFisher Scientific Inc, USA) was used as a marker for lysosomes in live cells.

4.2.5 TEM studies of intracellular trafficking

TEM studies were performed with ND internalized MDA-MB-231 cells for (24-120h). Cells were fixed at each respective time point. A routine cell sample preparation protocol for TEM was followed. Cells were fixed with 5% glutaraldehyde in s-collidine buffer and postfixed with 2% OsO_4 containing 3% potassium ferrocyanide, followed by successive steps of dehydration with ethanol and flat embedding using the 45359 Fluka Epoxy Embedding Medium kit. Thin sections of approximately 100 nm were prepared and stained with heavy metals (uranyl acetate and lead citrate). TEM microscopy was performed with an 80 kV JEOL JEM-1400 Plus (Joel Ltd, Japan).

4.3 Evaluation of NDs as a correlative microscopy probe

NDs are electron dense (TEM detectable) and photostable optical markers for fluorescence microscopy[56,76]. We evaluated the performance of NDs as nanosized dual markers for correlative microscopy. NDs were incubated with MDA-MB-231 cells for 24h. ND internalized cells were processed for TEM imaging following

routine sample preparation. Thin 100 nm sections were placed over marker EM grids. After TEM imaging, the cell section was placed over glass over coverslip and mounted over glass slide for imaging. The TEM imaged section was imaged with a TCS SP5 STED microscope (Leica microsystems, Germany). The NDs were excited with a 532 nm pulsed laser and PL was depleted with a STED beam at 765 nm. The emission was collected with an avalanche photo diode (APD) detector at the 665-705 nm range. Further, the SuperTomo software was applied for the automatic correlation of TEM and STED images[183].

4.5 siRNA delivery by MSN

4.5.1 Slow and sustained release of siRNA

The slow and sustained release of siRNA from the mesoporous of MSN nanocarriers was observed with live cell confocal microscopy (Paper V). Alexa 555 fluorescently labeled siRNA (BLOCK-iT™ Alexa Fluor® Red Fluorescent Control, Life Technologies, US) was loaded in FITC conjugated-MSN nanocarriers. The intracellular release of siRNA was observed in MDA-MB-231 cells for 96h. siRNA release in live cells was measured with TCS SP5 (Leica microsystems, Germany). The MSN nanocarriers (FITC conjugated) were excited with a 488 nm argon laser and the Alexa 555 labeled siRNA was excited with a 561 nm HeNe diode laser. The emission from thre MSN nanocarriers and the siRNA was collected at 510-540 nm and 570-610 nm, respectively. A co-localization study of the MSN and siRNA signals was performed with the Volocity® 3D Image Analysis Software (Perkin Elmer).

4.5.2 siRNA transfection efficiency

The transfection efficiency of the MSN nanocarrier's was evaluated with the WST-1 cell viability assay, colony growth monitoring by IncuCyte and a colony growth assay (Paper V)[175]. The transfection and gene knockdown efficiencies were evaluated with the commercially available AllStars Hs Cell Death Control siRNA (Qiagen, Germany). A 50 nM concentration of the AllStars Hs Cell Death Control siRNA was added to the MSN nanocarrier samples and the equivalent of AllStars Hs Cell Death Control siRNA was transfected with Lipofectamine® RNAiMAX (Invitrogen, Thermo Scientific, MA, USA). The transfection efficiency of the MSN nanocarriers was evaluated in comparison to Lipofectamine® RNAiMAX as a positive control.

5 Summary of the results

The nanoparticles studied in this thesis are summarized in Table 3.

Table 3. List of nanomaterials used in this study with surface functionalization and their respective studied applications.

Nanomaterials	Surface functionalization	Application	Publication No
I) Cancer cell imaging			
Nanodiamonds (NDs)	PEG, PEI	*In vitro* imaging	I
Nanodiamonds (NDs)		Intracellular trafficking, correlative microscopy	II-III
Nanographene oxide (nGO)	PEG, PEI, FA	*In vitro and In vivo* imaging	IV
Mesoporous silica nanoparticles (MSN)	PEG, PEI, FA	*In vivo* imaging	VI
II) Drug/siRNA delivery			
Nanodiamonds-silica composite (ND@MSN)	PEG, PEI	Drug delivery	I
Mesoporous silica nanoparticles (MSN)	PEI-Linker-PEI	siRNA delivery	V

The results of the cell imaging and drug/siRNA delivery applications are presented in two separate sections **I) Cancer cell imaging** and **II) Drug/siRNA delivery applications**.

I) Cancer cell imaging: Inherently fluorescent carbon nanoparticles (NDs and nGO) were evaluated for their suitability for *in vitro* (fixed cell) imaging (Paper I & IV). We studied the intracellular trafficking and cellular fate of NDs (Paper II). Further, NDs were used as dual probes for correlative light-electron microscopy (Paper III). nGOs and fluorescently labeled MSNs were evaluated for their feasibility for *in vivo* imaging using the chicken CAM model (Paper IV&VI).

II) Drug/siRNA delivery applications: For therapeutic delivery applications, we developed a potential multifunctional material with photoluminescent NDs (core)

and MSN as a shell, for the delivery of a hydrophobic model drug and its subsequent detection in cells[20]. The composite material (ND@MSN) was surface functionalized with PEI-PEG polymers and the cancer cell affinity ligand folic acid (FA) was attached to it (Paper I). Further, we synthesized and evaluated the suitability of MSN nanocarriers for the long-term (120h) delivery of siRNAs into cancer cells (Paper V). For this purpose, MSNs were designed by the integration of hyperbranched PEI and redox-responsive linker arms for the stimuli-responsive intracellular long-term sustained release of the siRNAs into the cancer cells.

5.1 Cancer cell imaging I

5.1.1 Inherently fluorescent nanodiamonds

The nanodiamonds used are photoluminescent (PL) and photostable markers suitable for cell imaging[184]. They have photostable and negatively charged PL nitrogen vacancies[56] in their lattice. However, the optical properties of the NDs are dependent on the type of synthesis and successful creation of negatively charged nitrogen vacancies[185]. ND production lacks a universal quality control procedure and quality might vary from batch to batch. Therefore, it's important to perform quality control tests for different batches of NDs. The NDs used in our evaluations were obtained from Tomei Diamond Co., Ltd (Japan) (Paper I). They were further irradiated with 2 MeV electrons to create nitrogen-vacancies. Irradiation of the NDs was performed as part of a collaboration at the General Physics Institute, Russian Academy of Sciences (Moscow, Russia) (Paper I).

We studied the morphology, size distribution, cytocompatibility and the potential of NDs for *in-vitro* cell imaging (Paper I). TEM was used to characterize their size and morphology. In general, NDs were typically below 100 nm in size. However, some NDs were smaller in size, roughly 30-40 nm **(Figure. 6a)**. TEM studies suggested that the NDs were irregular in shape. A cell viability assay was performed with the nanodiamonds, as a prerequisite assessment for biological applications. Cells treated with nanodiamonds (10 μg/ml) showed comparable viability to control cells (**Figure. 6b)**. We used a known cell toxin (Calyculin A) as a positive control for toxicity. In our experiments, NDs appeared non-toxic and the comparative cell viability can be seen in **Figure 6b**. We concluded that NDs were safe for further cell imaging application under our experimental conditions.

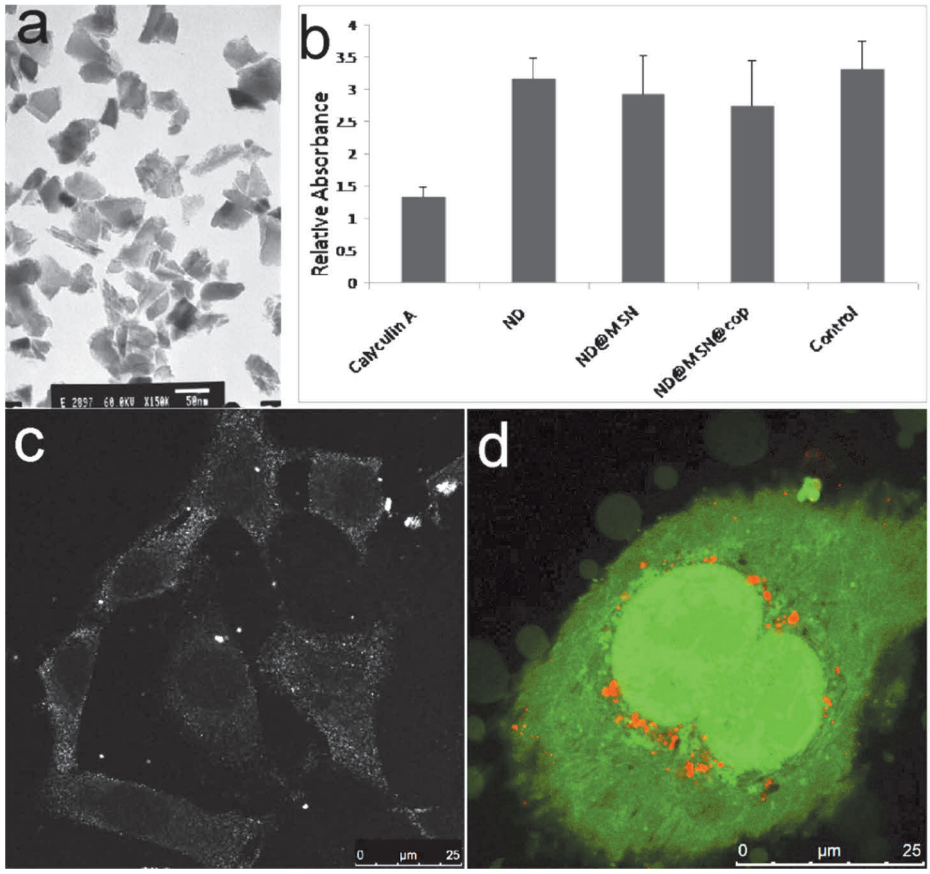

Figure 6. Nanodiamonds as photoluminescent probes for cellular imaging. a) Morphological and size characterization by TEM. b) Cytocompatibility assessment for ND and ND composites. Error bars represent standard deviation c) Cellular imaging of NDs in reflection mode. d) NDs as optical markers for cellular imaging. The PL signal from the NDs (red) can be seen localized to the cytoplasmic space of GFP expressing MDA-MB-231 cells (green).

Nanodiamonds were evaluated for their cellular imaging capabilities by confocal microscopy. We exploited both the refractive and PL properties of NDs. NDs have a high refractive index, and can be used for instance as optical markers for differential contrast microscopy. The scattered signals were bright enough to be distinguished from cellular autofluorescence **(Figure. 6c)**. However, optimal imaging settings are required for image acquisition in the reflection mode. Intracellular NDs were imaged with confocal microscopy in the fluorescence mode using an excitation wavelength of 488 nm and emission was collected at 650-730 nm. The PL from NDs (red) is an efficient optical probe for cellular imaging **(Figure. 6d).** Moreover, NDs were seen

to be localized in the cytoplasmic space and mostly in aggregates. The aggregated nature of the NDs suggests their endosomal confinement in the cells. However, further investigations were performed to understand the intracellular trafficking of NDs (Paper II).

5.1.2 Intracellular trafficking of nanodiamonds and investigation of cellular toxicity

Investigating the cellular interaction and fate of NDs could offer important insights into the material's biocompatibility. Despite the proven biocompatibility and efficient cellular internalization of NDs[60,119,184,186,187], diamonds are recognized as one of the hardest known non-biodegradable materials, and could thereby be toxic to cells. Clathrin-mediated endocytosis has been reported as the route of ND internalization into cells[119]. In a classical endocytotic process, the extracellular content moves primarily from early endosomes, mid-endosomes to late endosomes, and finally, vesicles merge with lysosomes as part of the degradation pathway[188]. Therefore, we investigated the localization of NDs with early endosomes and their interactions with lysosomes as a pre-state for exocytosis (Paper II).

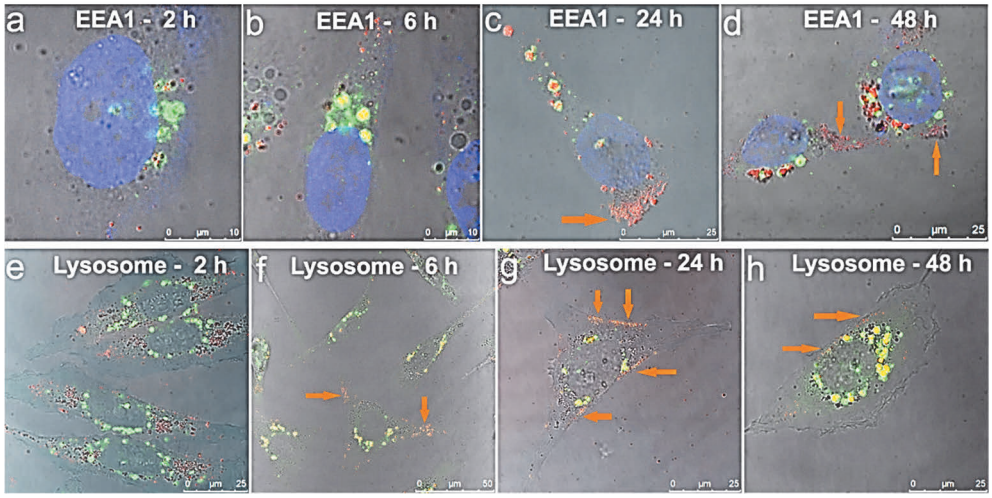

Figure 7. Continuous endocytosis and exocytosis of NDs can be interpreted from intracellular trafficking events. Investigation of NDs localized in early endosomes, as markers for cellular uptake. a) After a 2h incubation NDs (red) are localized within early endosomes (green), and in the cytoplasm. b) After 6 h, large aggregates of NDs were seen localized with early endosomes. While another ND population was observed to form smaller aggregates and can be seen more dispersed in cells. c) After 24 h, three distinct populations of NDs can be observed in cells: 1) Early endosomal localized NDs, 2) NDs mostly aggregated but they were not localized within early endosomes and 3) a dispersed, distinct ND population, which was mainly localized in close vicinity of the plasma membrane (arrow). d) After 48 h, the observation suggests that a small but significant population of NDs can be seen localized within early endosomes. The larger population of NDs was not localized within early endosomes but can be seen dispersed in proximity of the plasma membrane (arrow). Temporal regulation of NDs in cells by lysosomes. e) After 2h of internalization, NDs (red) can be seen localized outside lysosomes (green). f) After 6 h, a population of NDs (red) was observed to be co-localized with lysosomes (green). Another population seems to be aggregated, but not localized within lysosomes and some lysosomes are seen without any NDs. g) After 24 h, the observation suggests that one population of NDs was mainly aggregated and co-localized with lysosomes, while another distinct, dispersed ND population was observed mainly located at the edges of the plasma membrane. h) After 48 h, the observation suggested that there was progressive co-localization of NDs (red) with lysosomes (green). However, a distinct and dispersed population of NDs was consistently observed to be localized in proximity of the plasma membrane (arrow).

Nanodiamonds were observed after a 2h incubation to be internalized and localized within early endosomes **(Figure. 7a).** NDs were seen to localize in early endosomes forming large aggregates after 6 h of internalization. The size of the vesicular aggregates was approximately 1.5-2 μm as was observed by fluorescence microscopy.

Another ND population was observed not to be in early endosomes, and was mostly in the form of smaller aggregates and localized in a more dispersed fashion in the cytoplasmic space **(Figure. 7b).** After 24 h of internalization, we observed three distinct populations of NDs: NDs mainly co-localized with early endosomes, NDs aggregated but not localized with early endosomes and a spread-out, distinct population of NDs, which were mostly localized in the vicinity of the plasma membrane (arrow) **(Figure. 7c).** The size of early endosomes localized ND aggregates were comparable to that observed at 6h and 24h time points.

After 48 h of ND internalization, a small yet significant population of NDs was associated with early endosomes, while a larger population of NDs was not bound to early endosomes but remained either aggregated or dispersed in the proximity of the plasma membrane (arrow) **(Figure. 7d).** Investigation of the localization of NDs with early endosomes over 48h revealed the presence of different ND population in cells. Further, interactions between NDs and lysosomes were studied to understand the subsequent fate of the NDs.

We further investigated ND localization with lysosomes using the live cell LysoTracker dye. NDs were mostly localized outside lysosomes 2h after internalization and there was no observed co-localization of NDs with lysosomes **(Figure. 7e).** ND internalization after 6h showed a population of NDs co-localized with lysosomes. At the same time, there were other ND populations, which were also mostly confined but not co-localized with lysosomes. There was also the presence of lysosomes without any NDs **(Figure. 7f).** The observation at 24h suggests that one population of NDs was mainly confined and seen to be co-localized with lysosomes, while another ND population in the same cells was distinct, mostly dispersely located largely in proximity of the plasma membrane **(Figure. 7g).**

Progressive co-localization of NDs with lysosomes was observed at 48h. Another notable observation was the presence of NDs in the cytoplasmic space, but not bound to lysosomes. However, a significant population of NDs was localized again in proximity of the plasma membrane **(Figure. 7h).** The co-localization of NDs with lysosomes and early endosomes suggests that one significant population of NDs was either localized with early endosomes or lysosomes at the 6h, 24h, and 48h time points, while another significant ND population was mostly localized in proximity of the plasma membrane. These observations suggest that the localization of NDs

with early endosomes (2h, 6h, 24h, and 48h) can be interpreted as the continuous endocytosis of NDs in cells **(Figure. 7a-d)**.

However, continuous endocytosis of NDs and in the absence of exocytosis would finally lead to the accumulation of NDs in cells. This would certainly cause adverse effects on cell proliferation, growth and thus contribute to cellular toxicity. However, we have also observed, and it has been also reported, that NDs can act as a non-toxic nanomaterial in cellular studies. Similarity, considering the localization of NDs with lysosomes (2h, 6h, 24h and 48h), the observations at different time points suggest some degree of co-localization at each given time point. Therefore, it would be logical to hypothesize that the exocytosis and endocytosis of NDs occur simultaneously in cells. Cells could be using this endocytosis/exocytosis machinery to basically avoid the toxic effects of non-degradable NDs (Paper II).

Evidence of exocytosis was provided by NDs internalized into eGFP expressing MDA-MB-231 cells. ND containing eGFP MDA-MB-231 cells were co-cultured with other cancerous line (HeLa, non-GFP MDA-MB-231) and a non-cancerous cells lines (HSF, MEF).

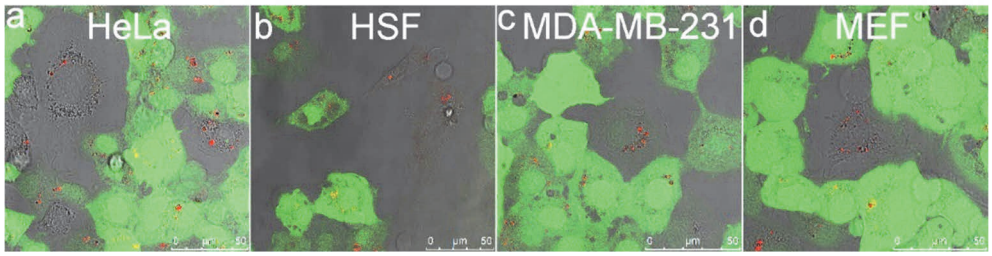

Figure 8. Demonstration of ND exocytosis from cells. eGFP MDA-MB-231 cells grown in the presence of NDs show exocytosis, and exocytosed NDs were internalized by cells in the co-culture. a) HeLa. b) HSF. c) non-GFP MDA-MB-231 and d) MEF cells.

eGFP expressing MDA-MB-231 cells were first cultured with NDs for 6 h to facilitate ND uptake. The culture medium was then changed to one not containing NDs, and HeLa, non-GFP MDA-MB-231, HSF or MEF cells were seeded into the co-culture. After 48h of co-culturing a significant ND population was seen in the co-cultured cells **(Figure. 8)**, suggesting the exocytosis of NDs from the eGFP MDA-MB-231 cells.

Furthermore, transmission electron microscopy was applied to visualize the sub-cellular localization of NDs and to observe vesicle bound and peripheral ND

populations. Earlier fluorescence microscopy experiments had showed the presence of different NDs populations in cells at various time points: either vesicle bound NDs (early endosomal and lysosomal) or NDs localized in the proximity of the plasma membrane. TEM imaging confirmed **(Figure. 9a-b)** that the localization of the NDs was mostly in a vesicular space (green arrow); as well as in proximity of the plasma membrane (orange arrow). The observation at 48h **(Figure. 9c-d)** suggests the progressive aggregation of NDs, mostly in a vesicular space. The observed vesicles were seen to be mostly packed with NDs and the sizes of the ND aggregates in the vesicles were approximately1-2 μm as seen by TEM **(Figure. 9c-d)**.

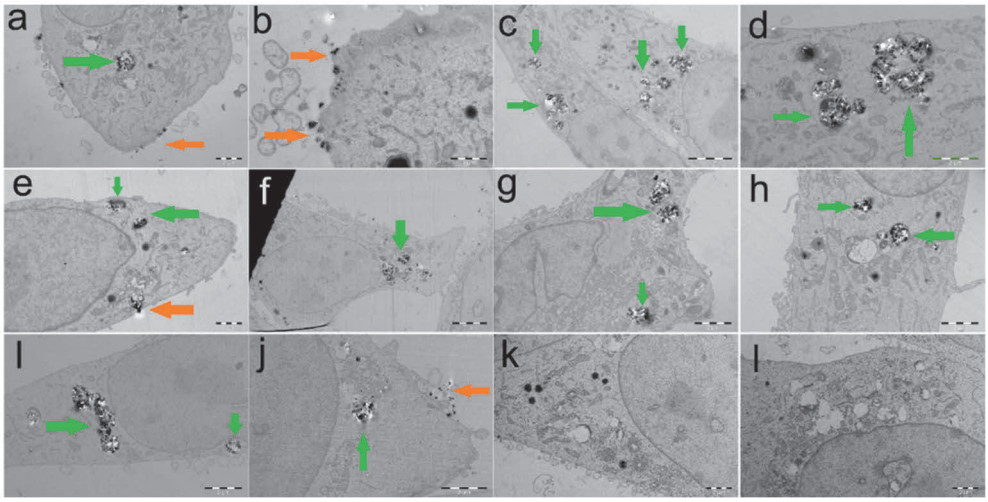

Figure 9. TEM imaging suggests vesicular localized NDs and NDs localized in the proximity of the plasma membrane. a-b) TEM imaging of NDs at 24h, suggest NDs localized in vesicles (green arrow) as well as in close proximity of the cell membrane (orange arrow). c-d) Vesicular aggregated NDs observed in cells at 48h. e) At 72h, TEM imaging shows an ND packed vesicle, which might be exocytosed from cells f) while NDs are confined in the vesicular space. Furthermore, vesicular aggregation was observed (g-h) at 96h. i) vesicular aggregated and j) NDs in the proximity of the cell membrane at 120h. k-l) empty vesicle seen in control cells.

It was observed (72h) that a NDs packed vesicle might be exocytosed from the cell **(Figure. 9e)**. The ND packed vesicle was confined on the edge of the plasma membrane **(Figure. 9e)**. However, other ND containing vesicles remained aggregated at 72h **(Figure. 9f)**. There were similar observations of NDs localized in a vesicular space at 96h and 120h **(Figure. 9g-j)**. TEM observations also concluded that NDs were not

localized in nuclei, mitochondria or Golgi. Vesicular localized NDs were aggregated and distinct from the empty vesicles of control cells **(Figure. 9k-l).**

TEM imaging revealed two distinct ND populations: one confined in a vesicular space, and the other mostly in the proximity of the plasma membrane. Taken together with the fluorescence microscopy study, the experimental observations suggest that substantial populations of cellular NDs were confined within early endosomes and lysosomes (6h, 24h, and 48h). These observations imply that cells could be managing the intracellular amount of NDs by continuous endocytosis and exocytosis. This could be a possible mechanism for cells to overcome the toxic effects of non-degradable NDs (Paper II).

5.1.3 NDs as a correlative STED-TEM microscopy probe

There is an evident need for a single fluorescent and electron dense probe for correlative light and electron microscopy (CLEM)[189]. Dual-contrast landmarks are required to match the details in the multi-modal images. CLEM allows combining the advantages of light and electron microscopy[190,191]. Fluorescence microscopy can be employed to study specific details in live or fixed cells. Subsequently, cells can be fixed and further studied with TEM. TEM allows the study of the ultrastructural details of cells at high-resolution. However, there is a resolution gap between TEM and fluorescence microscopy. In recent decades, with the development of super-resolution fluorescence nanoscopy methods, the resolution mismatch has been alleviated but not completely removed. The technology used here, Stimulated Emission Depletion (STED), is a super-resolution fluorescence microscopy technique, based on point-scanning confocal microscopy[75].

NDs, as mentioned above, are made of an inherently fluorescent, photostable and electron dense material[56,60,185,187], and NDs are compatible with the STED technique. NDs have been used as stable probes that can be efficiently resolved by STED microscopy down to 6 nm[76,85]. The electron dense nature of NDs allows them to be detected also by TEM **(Figure 6a)**. Therefore, NDs were applied as a dual contrast probe for STED-TEM correlative microscopy (Paper III).

Preparing cells samples for TEM involves harsh treatments with chemical fixatives such as Glutaraldehyde, 2% OsO_4 containing 3% potassium ferrocyanide and it also requires heavy metal staining to allow detection with the electron microscopy

(uranyl acetate and lead citrate). As a result of the severe chemical treatments, traditional organic fluorophores do not survive and hence cannot be further detected by fluorescence microscopy. However, NDs remained fluorescent even after the strong chemical fixation and heavy metal staining used in TEM sample preparation (**Figure. 10a-c**). As can be seen in **(Figure. 10d-f),** TEM processing does not appear to harm the fluorescent properties of the NDs and they can be subsequently imaged with fluorescence microscopy (**Figure. 10d-f**).

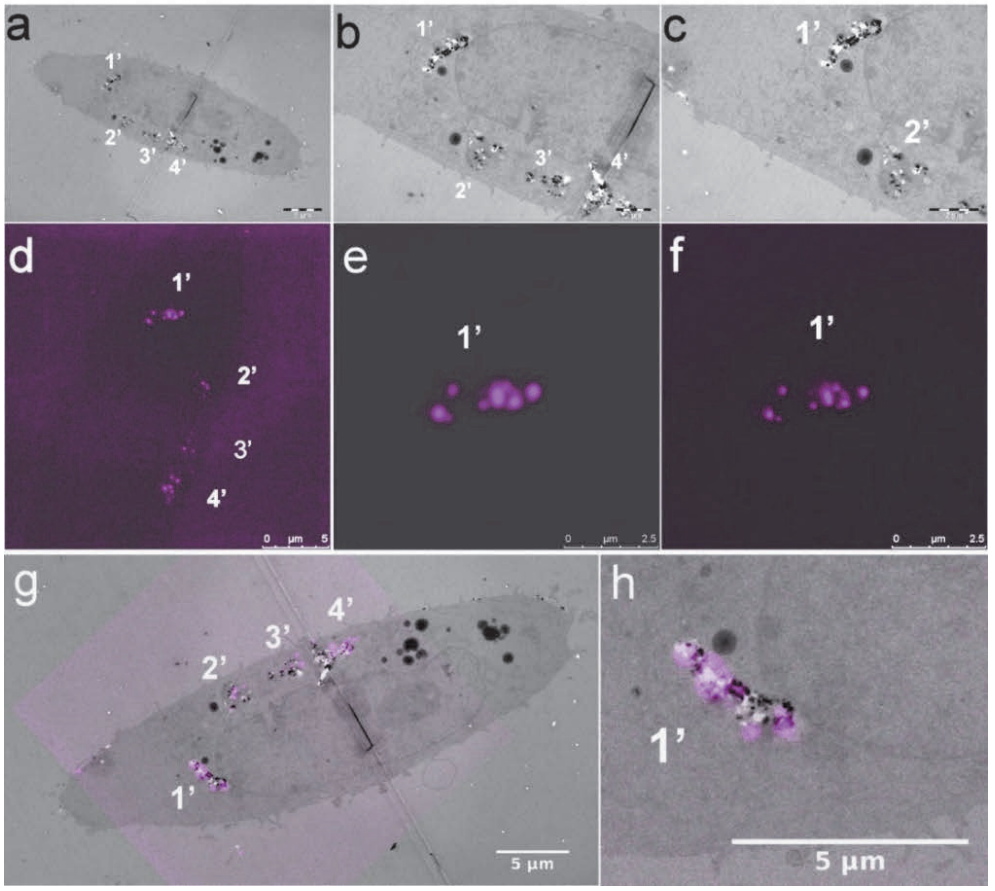

Figure 10. Nanodiamonds as dual contrast probes for STED-TEM correlative microscopy. a-c) TEM imaging of a cell with 4 distinct endosomal localizations of NDs. d) STED imaging of intracellular nanodiamonds. e) Confocal imaging of NDs localized at spot 1. f) STED depletion improves the overall resolution and precise localization of NDs in cells at spot 1. g-h) Correlative STED-TEM of the cell using nanodiamonds as an intracellular probe for both modalities.

Further, STED depletion could be used to resolve the NDs at optical super-resolution (**Figure. 10f**); where the resolution was evaluated from the distance of two NDs to be < 100nm. SuperTomo was used to correlate the multi-modal images[183](**Figure. 10g-h**). The NDs enable the precise mapping of the high-resolution structural details shown in TEM, with the fluorescence image obtained with STED **(Figure. 10g-h)**. NDs did not display photobleaching in our experiments, and they provided a strong intrinsic contrast in CLEM (Paper III). This is an additional advantage of NDs, to their previously shown potential applications for cellular imaging.

5.1.4 Nanographene oxides as inherently fluorescent carbon probes

Nanographene oxides (nGO) are a type of carbon based nanostructures[192]. nGOs have tuneable PL properties that are attractive for cell imaging, e.g. low toxicity and stable PL[192,193]. The nGO used in our study was synthesized by oxidizing micro- and /or nanographite in a 3:1 ratio of sulfuric to nitric acid (SNOx) (Paper IV)[122].

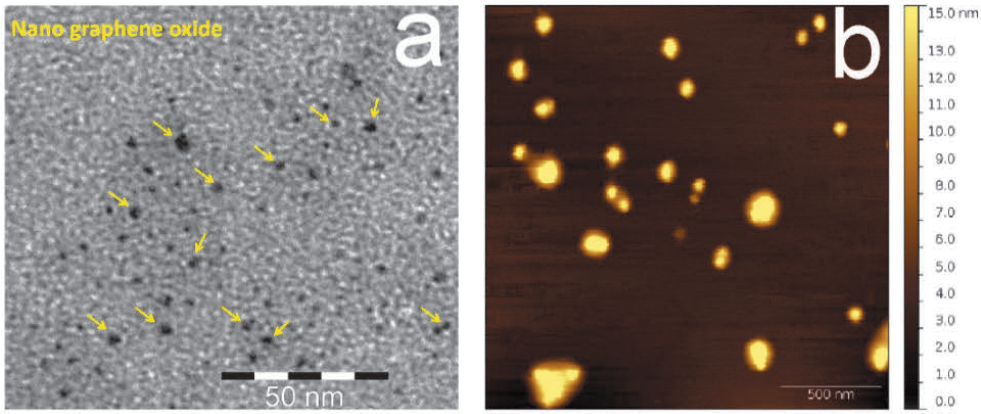

Figure 11. Investigation of the size distribution of nGOs by transmission electron microscopy (TEM) and atomic force microscopy (AFM). a) TEM imaging of nGOs. b) Atomic force microscopy of nGOs. nGO nanoparticles.

TEM and AFM were applied to study the size distribution of nGOs. The nGO particles were mostly below 10 nm in size. (**Figure. 11a**). We further applied AFM to investigate the size distribution of the nGOs. AFM data showed a similar of size distribution (**Figure. 11b**).

Table 4. Nanographene oxide (nGO) particles used in the study with surface functionalization**.**

Nanographene oxide nanoparticles	**Applied surface functionalization**
nGO	Uncoated
nGO-Cop	Coated with PEG-PEI (Cop)
nGO-Cop-FA	Coated with PEG-PEI (Cop) and attached with affinity ligand FA (Folic acid).

The optical properties of nGO, nGO-Cop and nGO-Cop-FA were characterized with spectrofluorimetry. nGO (coated and uncoated) has shown excitation-dependent emission over the entire visible spectrum (Paper IV). Multiple optical centers were observed with nGOs and emission maxima were observed at approximately 70-90 nm from the excitation wavelength[123]. A comparative spectrofluorometric analysis of nGO, nGO-Cop, nGO-Cop-FA nanoparticles was performed by exciting at 405 nm, 488 nm and 532 nm (**Figure. 12a-c**).

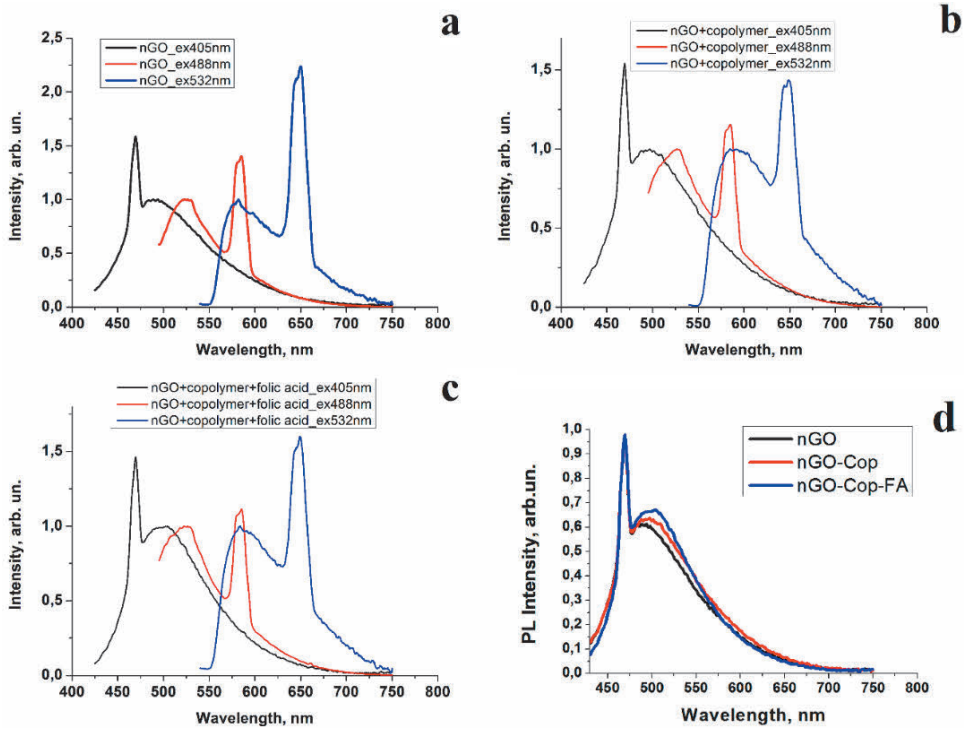

Figure 12. Surface functionalization of an nGO improves its photoluminescent properties. The observation of excitation-dependent emission spectra of nGOs (coated and uncoated) nanoparticles. a) nGO (uncoated). b) nGO (copolymer). c) nGO (co-polymer and folic acid). Effect of surface functionalization (Cop and Cop-FA) on the quantum efficiency of an nGO. d) Improvement in the quantum efficiency of a coated nGO (Cop and Cop-FA) over an uncoated nGO. The emission maxima were seen to red-shift in the following way: λ^{PL}_{max} *(nGO) = 489 nm,* λ^{PL}_{max} *(nGO-Cop) = 497 nm,* λ^{PL}_{max}*(nGO-Cop-FA) = 504 nm. e)*

It was critical to evaluate the quantum efficiency with or without organic surface functionalization. Surface functionalized nGOs (PEG-PEI) co-polymer, nGOs (PEG-PEI-FA) exhibited improved quantum efficiency over non-coated nGOs under similar conditions (**Figure. 12d).**

Table 5. Determination of the quantum yield for coated and non-coated nGOs. The quantum yields for nGO, nGO-Cop, nGO-Cop-FA were 4.8%, 6.2% and 7.1% respectively.

Parameters	**nGO**	**nGO-Cop**	**nGO-Cop-FA**
Concentration	0.01 mg/ml	0.01 mg/ml	0.01 mg/ml
Quantum yield	4.8 %	6.2 %	7.1 %
F_0 (λ_{exc}=405 nm)/max_{PL}	15.8 / 493 nm	16.1 / 498 nm	17 / 501 nm
F_0 (λ_{exc}=488 nm)/max_{PL}	5.3 / 527 nm	7.7 / 528 nm	8.7 / 528 nm
F_0 (λ_{exc}=532 nm) /max_{PL}	3.2 / 588 nm	5.4 / 589 nm	7.6 / 590 nm

Consequently, organic functionalization enhances quantum efficiencies along with providing better colloidal stability and presumably plays an important role in cellular applications, as discussed previously.

The cell viability of each separate surface modification using different concentrations of nGO nanoparticles with HeLa cancer cells was thus evaluated.

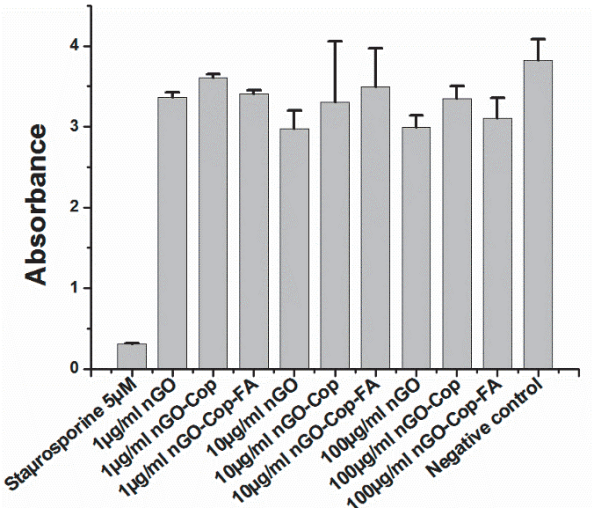

Figure 13. Demonstration of the biocompatibility of nGOs for cellular applications. A WST-1 cell viability assay was performed by increasing the concentration of the nGO particles with different surface functionalizations 10-fold. The final cell population in each treatment was directly proportional to the absorbance values. Negative control cells were untreated and positive control cells were treated with 5 μM staurosporine (toxin), a known inhibitor of kinases. The cell viability was observed to be high, even at nGO concentrations of up to 100 μg/ml. Error bars represent standard deviation.

The viability cells incubated with nGO particles with different surface functionalization exhibited similar cellular viability in comparison to negative control cells. The viability of the nGO-incubated cells was observed to be very high in comparison to cells treated with Staurosporine (a toxin) after 48h. Consequently, we concluded that there was no visible cytotoxicity observed with nGOs or their surface functionalized derivatives **(Figure. 13).** The biocompatibility evaluation showed that nGOs are safe for cellular applications even at higher concentrations (100 μg/ml).

The optical detectability of nGOs (surface coated and uncoated) for cell labeling was compared and evaluated by confocal microscopy. We observed bright PL from surface-coated nGOs (PEG-PEI-FA) as compared to uncoated nGOs **(Figure. 14a-f)**. The PL was detected throughout the cytoplasmic space, thus suggesting that the nGO particles were efficiently internalized by the cells. The nGO particles seemed to be compartmentalized in endosomes after endocytosis and formed intracellular aggregates of detectable sizes. In addition to the added benefits of improving the quantum efficiency **(Figure. 14)**, PEG-PEI co-polymers presumably facilitate cellular uptake[134,193,194] of nGOs. Since nGOs are negatively charged particles, the electrostatic adsorption of PEI contributes to the overall positive charge on the nGO surface, while the PEG part promotes the colloidal stability by steric stabilization under aqueous conditions[195]. The positive charge and colloidal stability of the nGOs improves their cellular uptake by promoting interactions with the negatively charged membranes of cells (Paper IV).

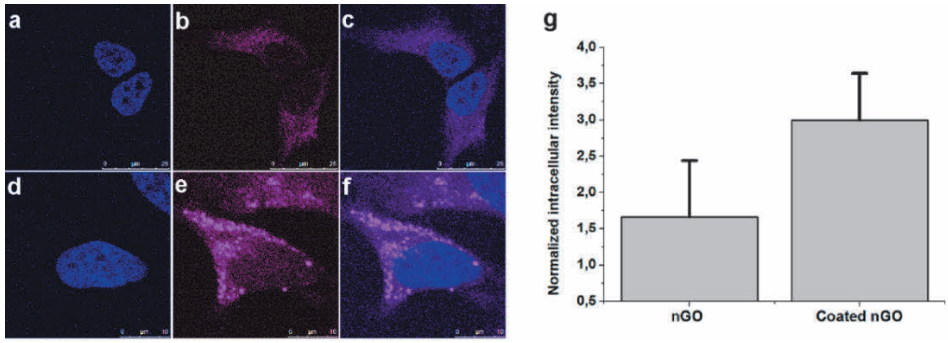

Figure 14. Effect of surface coating with PEG-PEI polymers with affinity ligands (Folic acid-FA) on cellular labeling for bioimaging. a) Hoechst stained nuclei of HeLa cells. b) PL from nGO (uncoated). c) Overlay. Surface coating promotes cellular uptake and enhances quantum efficiency thus improving the detectability of nGOs in cells. d) Hoechst stained nuclei of HeLa cells. e) Improved PL from coated nGOs in cells. f) Overlay. g) ImageJ based quantitative intracellular intensity analysis for nGOs (uncoated) and surface coated nGOs. Error bars represent standard deviation.

Furthermore, quantitative analysis of cellular uptake was performed with ImageJ by calculating the intracellular intensity of the signal **(Figure. 14g)**. Cell samples with both nGOs and nGOs (coated) were imaged with a confocal microscope using the same setting for quantitative comparison. The intracellular intensity analysis suggested that the uptake of the coated nGOs was improved by almost 100%

compared to uncoated ones. Therefore, the overall results suggest that the surface functionalization of nGOs significantly improves their PL and cellular internalization.

5.1.6 Evaluation of optical probes for cell tracking over an *in vivo* CAM model

The *ex-ova* version of the chicken chorioallantoic membrane model (CAM)[182,196,197] was selected as an animal model for *in vivo* imaging (Paper IV & VI).

Table 6. Nanomaterials with surface functionalization and their applications for in vivo imaging.

Nanomaterials studied for *in vivo* imaging	**Surface functionalization**	**Application**
nGO-Cop-FA	Coated with PEG-PEI (Co-polymer) and attached with affinity ligand FA (Folic acid).	*In vivo* imaging of labeled cancer cells
MSN-Cop-FA	Coated with PEG-PEI (Co-polymer) and attached with affinity ligand FA (Folic acid).	*In vivo* imaging

The *ex-ova* (shell less) version of the CAM (chorioallantoic membrane) model provided an optically transparent *in vivo* model with a large surface area and ease of tumor implantation **(Figure. 15a)**. Therefore, the non-invasive *in vivo* imaging of cancer cells labeled with nGO-Cop-FA particles was performed to demonstrate the potential of nGO as a stable optical probe (**Table. 6**). The *ex-ova* model offered easy access to microvasculature and easy implantation of nGO-Cop-FA labeled tumor cells **(Figure. 15b).**

The shell of the fertilized egg was carefully removed and its contents were placed in a weighing boat **(Figure. 15a).** Cancer cells with functionalized nGOs, as a PL marker were implanted over the CAM **(Figure. 15b).** The nGO labeled cancer cells were allowed to grow for one week to form tumors **(Figure. 15c).** The nGO labeled cancer cells (HeLa, A549, and MDA-MB-231) (**Figure. 15d-f**) were bright and detectable, even after 1 week of cell implantation. The nGO labeling allowed the detection of implanted cells, with a low laser power, without any noticeable damage to cells or vasculature.

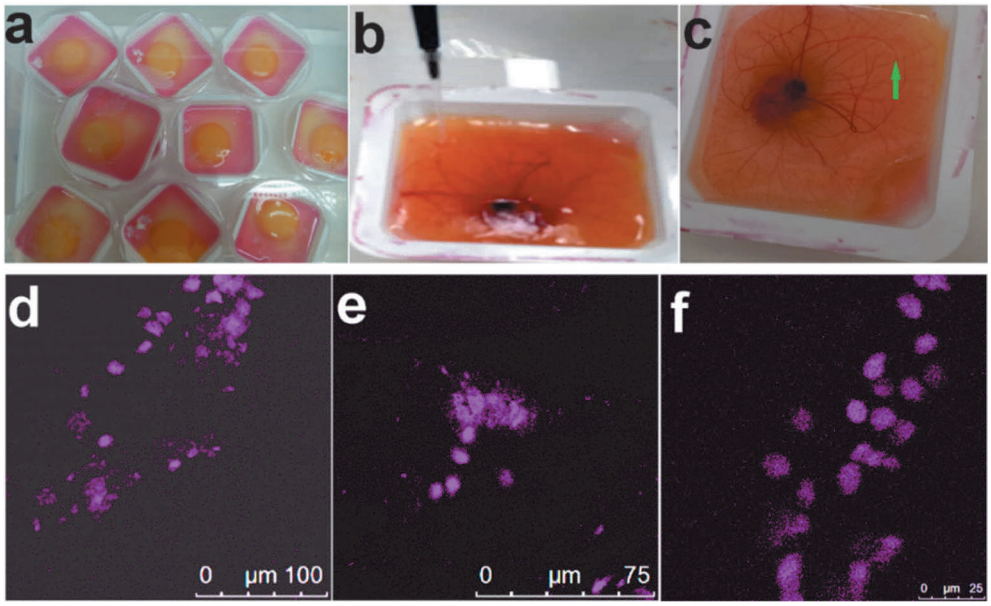

Figure 15. Surface functionalized and affinity ligand attached nGOs (PEG-PEI-FA) as an optical probe for in vivo imaging. a) Ex ova (shell less) CAM model. The large surface area with plenty of vasculature allows implantation of cancer cells. b) Implantation of cancer cells over the ex-ova CAM model. c) nGO labeled tumor. Multi-photon microscopy allows imaging of nGO labeled tumors after 1 week of implantation (arrow). d) HeLa cells. e) A549 cells. f) MDA-MB-231 cells. The two-photon imaging parameters were MP Ex. 800nm, Nondescanned detector Em.430-480nm, 20X dip objective.

Fluorescently labeled MSNs were also evaluated for their *in vivo* detectability in the CAM model (Paper VI). The *in vivo* imaging of MSNs was performed by injecting them into the blood vessels of the chick embryo CAM **(Figure. 16)**. MSNs were surface coated with the PEG-PEI copolymer, and the affinity ligand FA was attached to them (Table.6). Further, MSNs were conjugated with the fluorophore rhodamine.

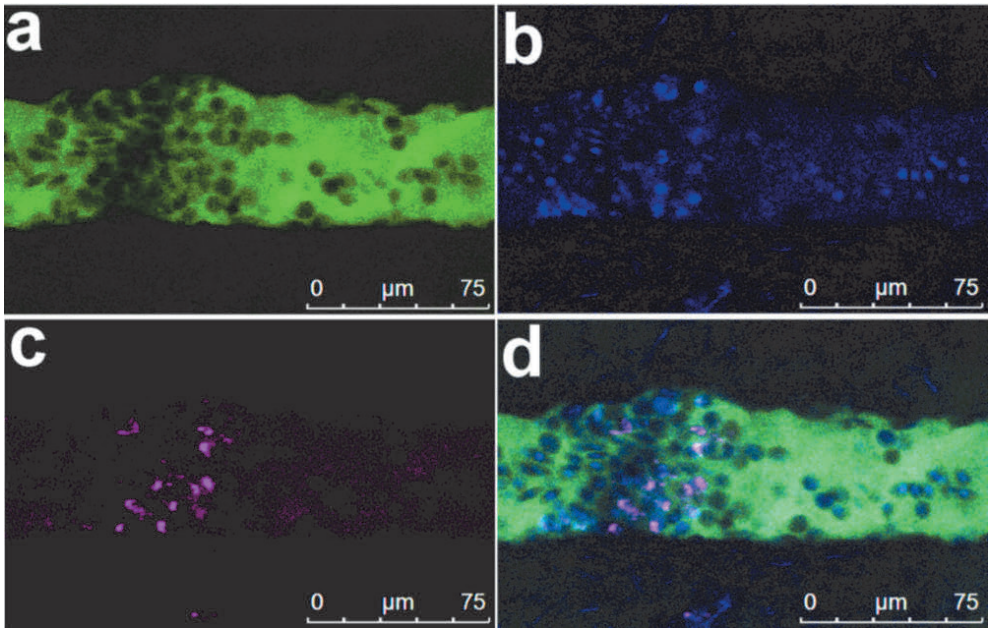

Figure 16. In vivo imaging of circulating MSN nanoparticles coated with a copolymer, and with an attached affinity ligand, folic acid (FA) in blood vessels of the chicken embryo. a) blood vessel (FITC dextran labeled). b) Nuclei (Hoechst labeled nuclei). c) Detection of circulating MSN-Cop-FA nanoparticles in blood vessels. d) Overlay image.

The CAM model provided the technical simplicity needed to understand the biological behavior of MSN in an *in vivo* environment and the optically transparency allowed imaging (two-photon excitation) inside blood vessels **(Figure. 16)**. The MSN-Cop-FA nanoparticles were detectable, bright and stable under *in vivo* conditions. The MSN-Cop-FA‘s detectability and stability make it a potential candidate for the targeted and monitored intravenous delivery of drugs (Paper VI).

5.2 Drug / siRNA delivery II

5.2.1 Nanodiamond-silica composites as potential multifunctional probes

Having established the cellular imaging capability, cytocompatibility, cellular trafficking and morphological characteristics of NDs, as described above, we were interested in loading the NDs with drugs to test their broader applicability (Paper I). We fabricated a novel core-shell composite material using NDs as the fluorescent core and mesoporous silica as the outer shell (ND@MSN)[20]. NDs offer a limited surface area for delivery i.e. only the external surface area can be exploited for drug

adsorption. Mesoporous silica is a well-established versatile material for the delivery of drugs[19,137]. A mesoporous silica shell provides a large surface to volume ratio, allows the attachment of targeting moieties and functional organic groups; which can be further exploited for surface functionalization and a higher degree of cargo loading for drug-delivery applications[115,180]. Moreover, the photoluminescence originating from the ND core allows it to be subsequently imaged with cells. Therefore, the ND@MSN could be exploited as a potential multifunctional probe for drug-delivery and imaging (Paper I).

Table 7. ND@MSN with surface functionalization.

Nanomaterial for drug-delivery	**Surface functionalization**
ND@MSN	Core-shell composite of nanodiamond (core) with silica shell.
ND@MSN-Cop	Core-shell nanodiamonds silica composite surface functionalized with PEG-PEI Co-polymer coated

Coating NDs with a silica shell also provided a regular shape and helped minimize aggregation. TEM imaging of the novel composites revealed the ordered pores of the silica and the ND localized in the core **(Figure. 17a)**. We investigated the comparative drug loading capacity for NDs, ND@MSN composites, and ND@MSN-Cop. The dye DiI, a lipophilic, plasma membrane non-permeable hydrophobic molecule, was selected as the cargo molecule to study the drug loading capacity of the composites and the subsequent intracellular release of the dye. Thus, the designed delivery system could also facilitate the intracellular delivery of poorly water-soluble drugs, especially non-lipophilic compounds that show low permeability into biological membranes. However, the delivery system could also be used as a carrier for liquid or semisolid forms of lipophilic drugs, also for purposes other than intracellular delivery[198]. The dye adsorption study concluded, that full adsorption of the DiI dye (2.5wt %) was observed with hybrid composites, whereas with NDs an absorbtio of only 0.5wt% was reached[60]. Some non-significant leaching of the DiI dye was observed with all samples during co-polymer coating, which was conducted under aqueous conditions. Hence, coating NDs with silica vastly improves their drug loading capability.

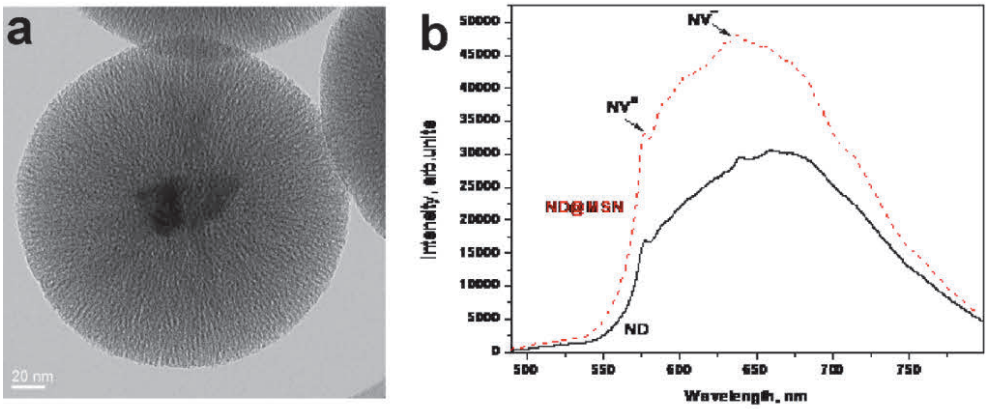

Figure 17. Characterization of the morphology and PL properties of ND@MSN (hybrid composites). a) High-resolution TEM imaging of ND@MSN. The ordered pores of the mesoporous silica shell can be seen with the ND as the core. b) Silica coating over NDs had no adverse effects on the PL properties of NDs. Zero-phonon lines of NV^{o} (neutrally charged) and NV^{-} (negatively charged) optical centers are shown by arrows at 576 nm, and 639 nm, respectively.

We performed a PL spectra analysis of NDs and ND@MSN at a 488 nm laser excitation. The observations suggest that there are no adverse effects on the PL properties of NDs due to the silica coating (ND@MSN). On relative terms, the increase in photoluminescence appears to be more than 'slight' **(Figure. 17b)**.

ND@MSN-PEI-PEG were expected to promote the efficient delivery of loaded cargo along with maximizing delivery to a population of cells. The obtained results suggest that ND@MSN-PEI-PEG could successfully permeate across the cell membrane, without showing any particle aggregation, and no premature release of content **(Figure. 18a)**. On the contrary, ND@MSN tended to form large aggregates and were not able to cross the plasma membrane, thus leading to unsuccessful delivery of hydrophobic model drugs **(Figure. 18b)**. The observed results imply the importance of surface functionalization of ND-based carriers for drug delivery and cellular internalization (Paper I).

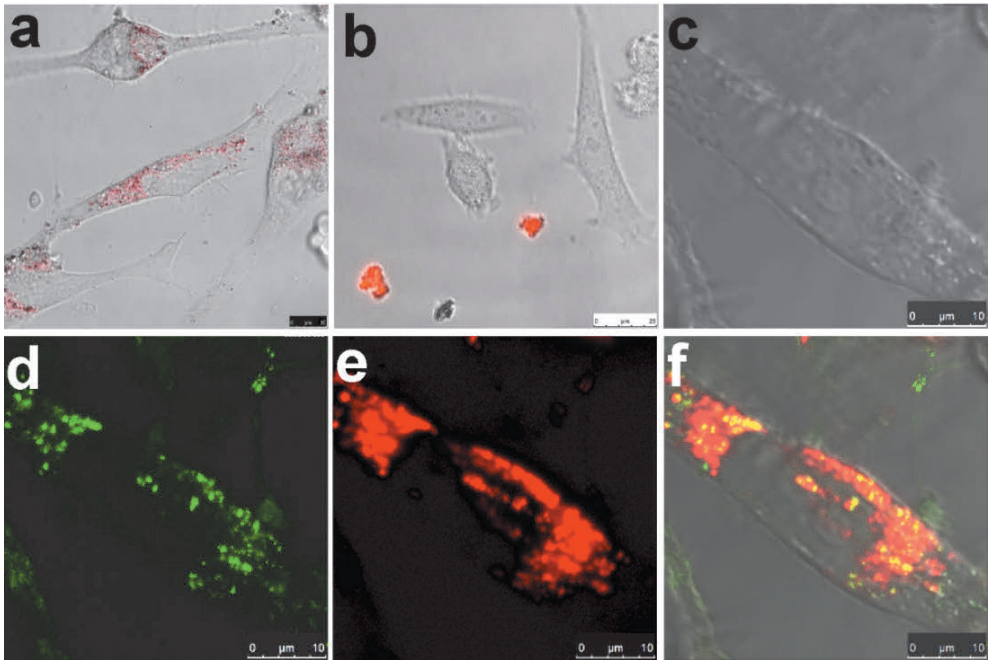

Figure 18. Intracellular drug delivery by ND@MSN and effects of surface functionalization (co-polymer) for delivering the hydrophobic model drug. A co-polymer (PEI-PEG) coating over ND@MSN facilitates cellular uptake, prevents premature release of cargo and prevents aggregation of hydrophobic drugs. a) Successful internalization of DiI loaded ND@MSN. b) Aggregation of uncoated ND@MSN. The intracellular release of DiI and subsequent imaging with the multifunctional ND@MSN@PEI-PEG. c) A bright field image of d&e. d) PL originating from ND cores, suggests endosomal localization, e) while the release of DiI observed throughout the cytoplasm suggests endosomal escape of the cargo. f) The co-localization of the ND signal with DiI indicates the successful intracellular release of DiI.

Upon the successful internalization of ND@MSN-PEI-PEG, significant amounts of intracellular release of cargo were observed in the cells **(Figure. 18c)**. NDs were seen localized in an aggregated fashion, suggesting endosomal trapping **(Figure. 18d)**. As can be seen, the DiI dye was spread out throughout the cytoplasm **(Figure. 18e)**. The co-localization of the ND signal with DiI (yellow) is indicative of the successful intracellular release of DiI (red) **(Figure. 18f)**. The results suggest that ND@MSN-PEI-PEG could be a potential system for the efficient intracellular delivery of poorly water-soluble drugs.

5.2.2 siRNA delivery

RNAi using siRNAs is a promising and a highly potent mechanism for selectively inhibiting specific genes[37,40]. However, it is challenging to protect the siRNAs from

degradation and to deliver siRNAs in a sustained manner for long term gene-based therapy[40,199]. Therefore, we developed and evaluated an MSN (MSN-PEI-linker-PEI) based nanocarrier, in which hyperbranched polycations (PEI) were conjugated with intracellularly cleavable bonds for the long term sustainable release of siRNA **(Figure. 19)** (Paper V).

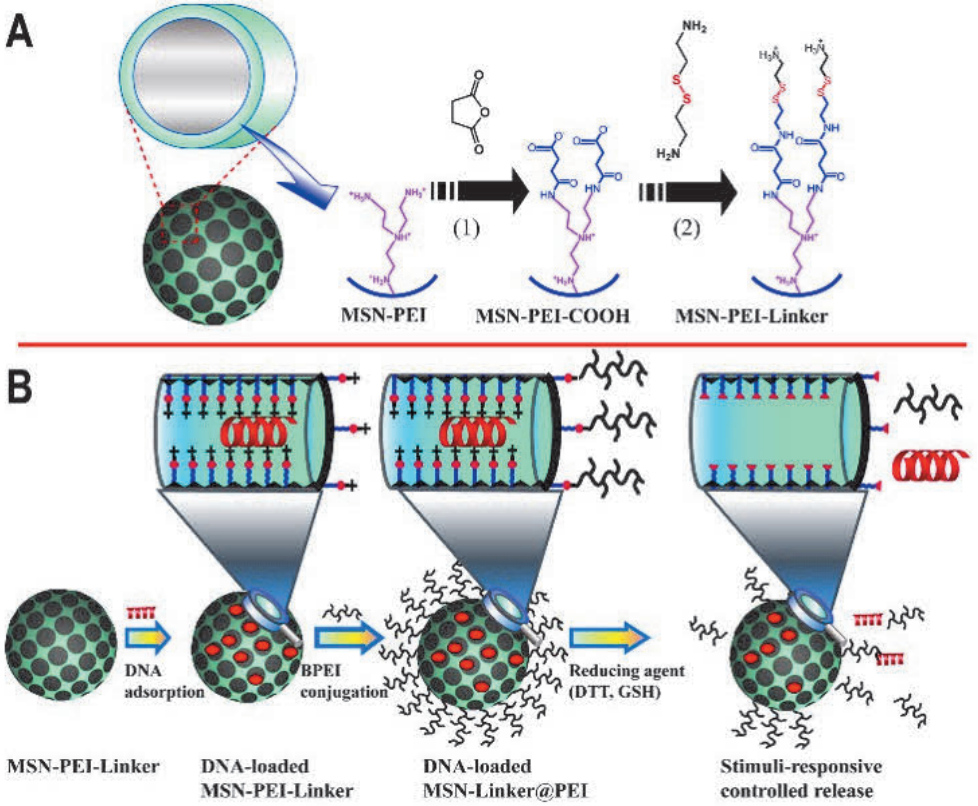

Figure 19. Schematic representation of the design of MSN nanocarriers (a) MSN pores were conjugated with the PEI polymer. a) Functional COOH groups were further attached to the PEI polymers. Further, intracellularly cleavable disulfide bonds (Linkers) were chemically attached. (b) Representation of siRNA loading. Negatively charged siRNAs were electrostatically attached to the positively charged, exterior PEI.

The cellular viability of MSN nanocarriers (without siRNA) was evaluated by the WST-1 assay. The results of the WST-1 assay showed that the viability of MDA-MB-231 cells incubated with the MSN nanocarriers incubated for 72h remained comparable to negative control cells and that no significant toxicity was observed with the MSN nanocarriers (MSN-PEI-linker-PEI). The results for lower MSN

nanocarrier concentrations (2 and 10 µg mL-1) suggest that the viability was almost similar to negative control cells **(Figure. 19)**.

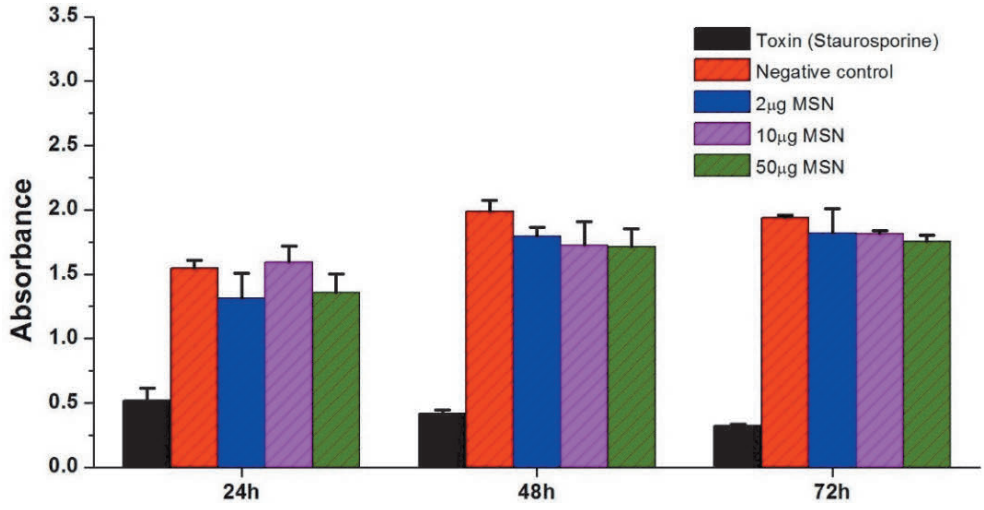

Figure 20. In vitro cell viability of MSN nanocarriers (MSN-PEI-linker-PEI) performed with WST-1 cell proliferation assay. Error bars represent standard deviation.

However, it is well established that a higher concentration of PEI could cause toxicity[200,201]. The WST-1 assay suggests that there was minimal toxicity associated with MSN nanocarriers at a higher concentration (50 µg mL-1). However, to avoid any toxic effects on cells, consequently, any further biological evaluations were carried out at a concentration lower than or equal to 20 µg mL-1 (Paper V).

The uptake of MSN nanocarriers was evaluated using MDA-MB-231 cells. FITC-labeled MSN nanocarriers (20 µg mL-1) were incubated for 24h and 48h. Confocal microscopy was applied to qualitatively analyze the uptake efficacy. The MSN nanocarriers were observed to be widely spread throughout the cytoplasmic space and the fluorescence signal from MSN nanocarriers was observed to come from be aggregated foci **(Figure. 21).** The fluorescence signal from MSN nanocarriers suggests that most of the particles were internalized within the first 24h **(Figure. 21c-e).** There was no significant increase observed in the fluorescence signal in cells 48h after the internalization of the MSN nanocarriers **(Figure. 21h-j).**

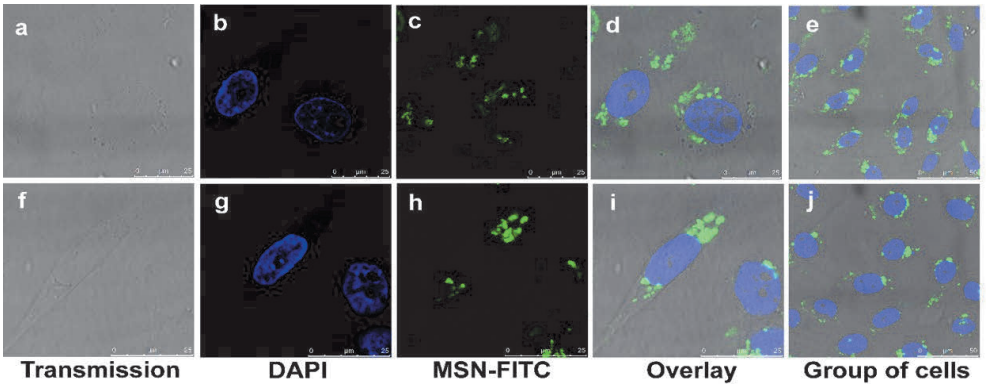

Figure 21. Internalization efficacy of MSN nanocarriers in MDA-MB-231 cells. a-e) uptake after 24 h of incubation. f-j) uptake after 48 h.

To evaluate and validate the newly designed MSN nanocarriers, we performed a long-term release study (96h) with live cell confocal microscopy **(Figure. 22)**. MSN nanocarriers were conjugated with FITC (green) and loaded with fluorescent siRNAs (Alexa-555 labeled siRNA), as a transfection control for slow and sustained release. Furthermore, the release of siRNAs from the MSN nanocarriers was quantified with the Volocity colocalization software based on Pearson's colocalization coefficient.

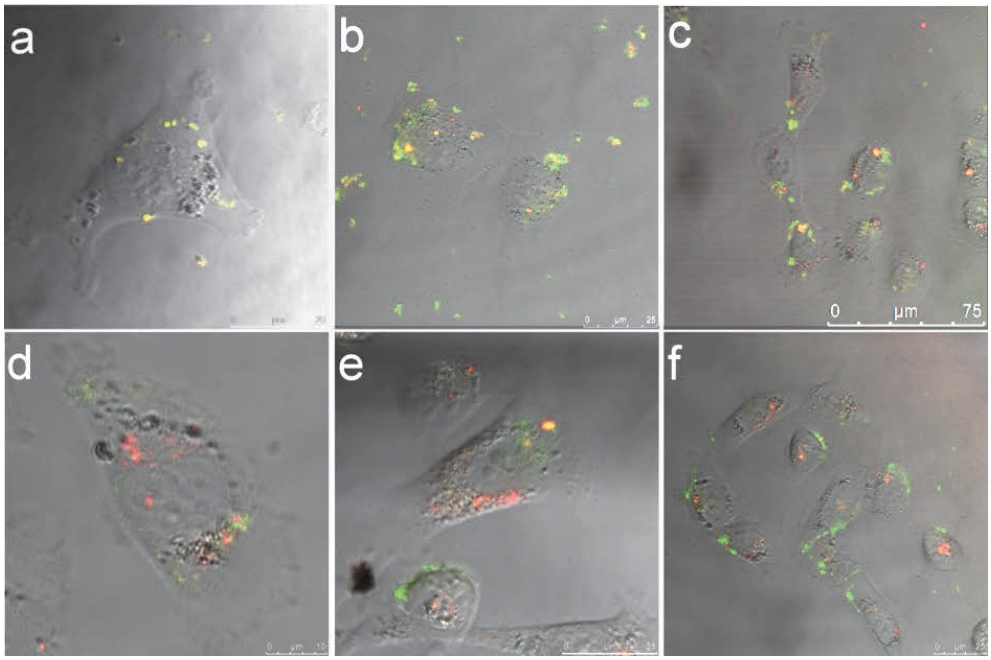

Figure 22. Slow and sustained intracellular release of siRNAs from MSN nanocarriers. We observed the progressive and sustained release of siRNAs (Alexa 555 labeled- red) from the pores of the MSN nanocarriers (FITC labelled-green). The intracellular release of siRNAs from MSN nanocarriers and the co-localization of the Alexa 555 and FITC signals over time at a) 0-2 h, b) 24 h, c) 48 h, d) 72 h and e-f) 96 h. The intracellular release of siRNA demonstrated that the fluorescence signals from the siRNA and MSN nanocarriers were mainly separated at 96 h. Thus indicating the slow and sustained release of siRNA into the intracellular space from the mesopores of MSN nanocarriers.

The initial observation at 0-2h shows the cellular internalization of MSN. We observed co-localized yellow fluorescent signals from the MSN nanocarriers (green) loaded with siRNA (red) (**Figure. 22a, 23**). The co-localized signal suggests that no premature release of siRNA was observed from the MSN nanocarriers. The co-localization at 24h, suggests that the MSN nanocarriers (with siRNA) were mostly intact and had not yet released their siRNA **(Figure. 22b)**. However, we observed the gradual increase (48h onwards) in distinct red fluorescence over time in the cytoplasm and the degree of co-localization was progressively lower at each successive time point (**Figure. 22c-f, 23**). Furthermore, a significant increase was observed in the green fluorescence, suggesting the partial release of the siRNA from the MSN nanocarriers (**Figure. 22c-f**). However, at 72h, live cell imaging suggested that some MSN nanocarriers still co-localized with siRNA in the cells. This might be

interpreted as the persistent and slow release of siRNA from the mesopores (**Figure. 22d**).

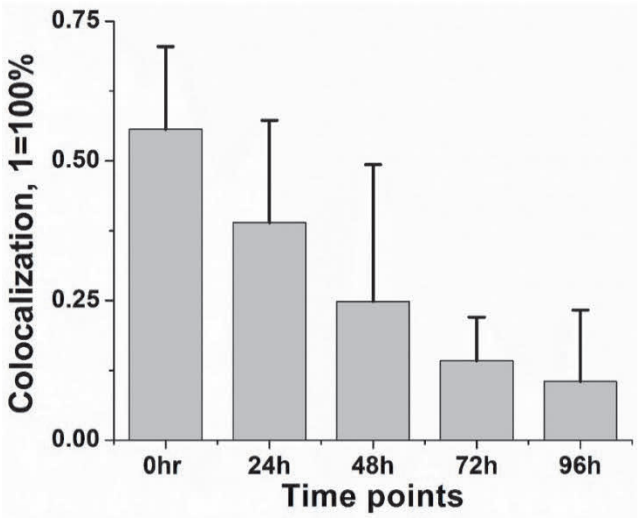

Figure 23. The degree of co-localization was quantified by calculating Pearson's correlation coefficient. The co-localization of the MSN nanocarriers and the siRNA fluorescence signal was observed to gradually decrease over time (0-96h), suggesting the sustained release of siRNA from the mesopores of the MSN nanocarriers. Error bars represent standard deviation.

Live cell imaging at 96h (**Figure. 22f)** shows well-separated fluorescence signals from the MSN nanocarriers (green) and the siRNA (red). siRNA release was observed to be more diffused as compared to the localized signal from the MSN nanocarriers. It was also observed that not all cells or all MSN nanocarriers exhibited synchronized release of the siRNA. Some cells exhibited more efficient release of siRNA than other cells. Based on the results above, it can be concluded that the MSN nanocarriers were efficient in delivering the siRNA intracellularly in a slow and sustained manner over a period of 96h, while protecting the siRNA from intracellular degradation for long term delivery **(Figure. 22)**.

The above siRNA release analysis with live cells suggested that 72-96h could be an optimal time for the efficient release of siRNA from our MSN nanocarriers. Therefore, to evaluate the gene knockdown efficacy of the MSN nanocarriers, 100-120h should be the ideal timeframe for achieving significant gene knockdown. To validate the transfection efficiency of the MSN nanocarriers, we used the commercial

AllStars Hs Cell Death Control siRNA, (Qiagen). The selected commercial siRNA was a blend of potent siRNAs, involved in the targeting of genes vital for cell survival[175,202]. The transfection efficacy of MSN nanocarriers was compared to a commercial transfection agent, Lipofectamine RNAiMax. It has an excellent transfection efficacy and is routinely used as an *in vitro* transfection agent.

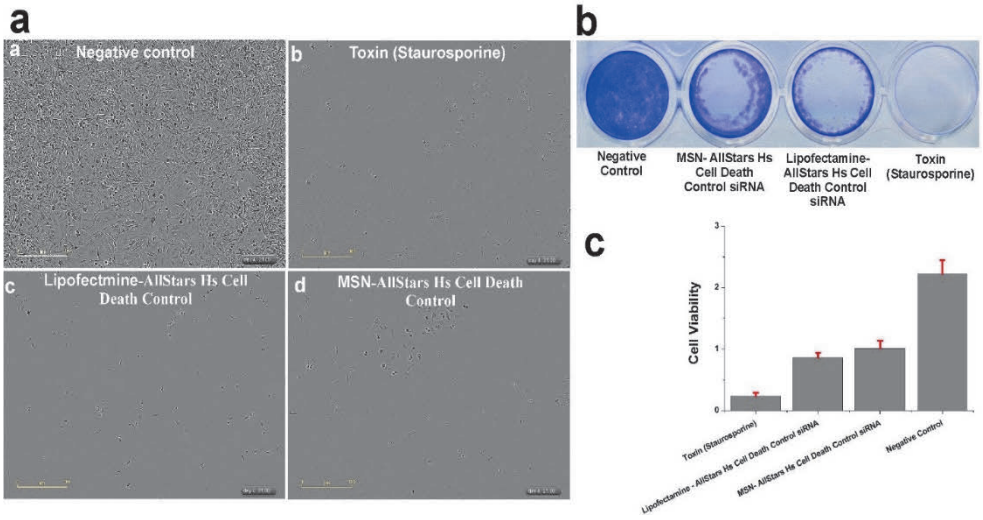

Figure 24. Gene knockdown efficiency of MSN nanocarriers evaluated by 1) Monitoring the growth of live cells 2) crystal violet staining and 3) WST-1 assay. Negative control cells were untreated and were observed to be confluent after 120h. Positive control cells were treated with staurosporine (cell growth inhibitor) and cells were mostly observed to be dead after 120h. MSN nanocarriers were found to be efficient in knocking down genes, as the inhibition of cell growth was observed. Lipofectamine RNAiMax served as a positive transfection control. a) Cell growth after 120h, MSN nanocarriers loaded with the AllStars Hs Cell Death Control siRNA. Live images with each treatment after 120 h (Figure 19a (a-d)). b) Cell viability as assessed by crystal-violet staining of cells at 120h. c) Cell viability assessed by the WST-1 assay after 120 h. Error bars represent standard deviation.

The RNAi functionality of MSN nanocarriers was experimentally evaluated by complementary techniques for determining cell viability 1) long term growth monitoring by IncuCyte ZOOM®, 2) crystal violet staining and 3) a biochemical assay (WST-1 assay). The evaluation with different techniques demonstrated that the MSN nanocarriers were efficient in delivering siRNA vehicles for gene knockdown **(Figure. 24)**. The experimental results can be summarized 1) nanocarriers have a demonstrated efficient protective effect on the loaded siRNA; 2) internalization is

followed by the endosomal escape of the siRNA; 3) the siRNA is released intracellularly in a sustained manner. Consequently, the developed MSN nanocarrier system includes the desired characteristics of a suitable vehicle for the *in vivo* delivery of siRNA. In summary, this study may bring a new outlook for designing vehicles for siRNA delivery and promote the understanding of host-cargo interactions for the further application of porous nanomaterials for the long-term delivery of siRNA (Paper V).

6 Conclusion and outlook

In this thesis, the suitability of fluorescent carbon-based nanoparticles (nanodiamonds and nanographene oxide), mesoporous silica nanoparticles and nanodiamond- silica composites, and their different surface modifications, were evaluated for applications in cancer cell imaging and drug / siRNA delivery.

Cancer cells were imaged with different *in vitro* and *in vivo* fluorescence microscopy techniques. Carbon-based fluorescent nanomaterials (NDs and nGO) can be efficiently applied for cell imaging as alternatives to organic fluorophores. They were shown to be non-toxic for cell labeling in our studies (PAPER I, IV). The intracellular trafficking studies of NDs suggested that cells manage the non-biodegradable material by continuous endocytosis and exocytosis. This provides additional information about the interaction of cells with nondegradable materials (PAPER II). Novel applications of NDs as CLEM labels promise to open up new opportunities for using the material in integrating advanced imaging systems such as electron microscopy and super resolution microscopy (PAPER III). In general, NDs are bright, electron dense, photostable and compatible with STED microscopy for cell labeling (PAPER I-III).

nGOs have shown to be efficient, stable and multi-color optical markers for cancer cell labeling. The results obtained in this study demonstrate the potential of nGOs as non-invasive *in vivo* optical imaging probes for the long term tracking of tumors in a model organism (PAPER IV). The nGOs have similar optical properties as quantum dots, however, their non-toxic nature brings added advantages for the long-term observation of cancer cell.

Surface modifications of nanoparticles possess great advantages for cellular imaging and drug delivery applications. In our studies, surface functionalization with PEG-PEI polymers and the attachment of an affinity ligand (folic acid) were shown to facilitate optical imaging and drug delivery. Surface functionalized NDs and nGOs showed higher cellular uptake and detectability than their non-modified counterparts (PAPER I & IV). In the case of nGOs, improved luminescence quantum efficiencies were observed with PEG-PEI-FA coating over uncoated nGOs (PAPER IV). The reason for the increase in quantum efficiency needs to be further investigated.

For drug delivery applications, the evaluated multifunctional composite (ND@MSN) with a PEI-PEG surface functionalization enabled cell imaging and the intracellular delivery of a poorly water-soluble model drug. The study emphasizes the application of dual purpose polymers (positively charged PEI and PEG for colloidal stability) for facilitating the delivery of hydrophobic drugs. The results obtained with a composite molecule with dual imaging and drug delivery properties represent a novel contribution to the development of multi-functional probes (PAPER I).

The delivery of siRNAs into cells remains challenging for many reasons. An ideal *in vivo* delivery system should offer advantages such as slow, sustained long-term intracellular delivery for an efficient knockdown. The presented MSN nanocarrier system has the potential of overcoming the main barriers associated with the delivery of siRNA. The developed system incorporates the positively charged hyperbranched PEI with intracellularly cleavable disulfide bonds (Paper V). The results can be concluded as follows: the newly developed MSN nanocarriers were internalized efficiently, they were biologically compatible and they performed the slow and sustained intracellular release of the siRNA for a prolonged time, while protecting the siRNA from degradation. Further, MSN nanocarriers can be applied to *in vivo* delivery, which is not possible with current commercial *in vitro* transfection agents. The MSN nanocarrier system showed an overall promising knockdown efficiency, which will prospectively empower more effective *in vivo* gene knockdown strategies for improved mRNA silencing by RNAi (Paper V).

The results presented in the thesis contribute new knowledge for the development of improved strategies for cancer cell imaging and drug-delivery. The role and effects of organic surface functionalization approaches have been broadly discussed in cancer cell imaging. The developed drug /siRNA delivery systems provide a glimpse of some solutions for the increasingly complex and challenging field of cancer drug/siRNA delivery systems. However, many aspects of cell imaging and the delivery system remain to be investigated before translational clinical applications can be designed.

Acknowledgements

This work was carried out at Pharmaceutical Sciences Laboratory, Åbo Akademi University in close collaboration with Laboratory of Biophysics, University of Turku. I would like to sincerely thank "The Doctoral Education Network in Materials Research (DNMR)", Åbo Akademi University for providing funding for successfully carrying out my PhD studies. I am also thankful to NGS Nano Graduate School and ÅÅ Foundation for providing travel grants for attending scientific programs.

I would like to express my gratitude toward Professor Niko Hildebrandt and Adjunct Professor Clare Strachan for reviewing my thesis and providing constructive suggestions to finalize my PhD thesis. I am in particular thankful to Professor Matthias Nees for agreeing to act as an opponent.

I would like to express my heartfelt gratitude to my supervisor, Professor Jessica M. Rosenholm, for providing an excellent opportunity to carry out my PhD studies. Jessica, thank you for providing an outstanding research atmosphere, autonomy, constructive suggestions throughout PhD studies. I am grateful to you for introducing me to the unique world of "nanomaterials". It's been a wonderful journey working with Bionanomaterials group; time spent here is going to be a treasure that would be cherished forever.

I would like to offer my sincere gratitude to my co-supervisor, Professor Pekka E. Hänninen, for providing an outstanding support, guidance and letting me be a part of Laboratory of Biophysics since my BIMA days. It's been a privilege to be introduced to the incredible world of "light microscopy". I will be forever thankful to you and Team "Biophysics" for continuous support during my PhD studies.

I would like to thank all the co-authors of the papers presented in the thesis. I am extremely thankful to all close collaborators Dr. Olga Shenderova, Prof. Huan Chang, Prof. Jukka Westermarck, Prof. Cecilia Shalgren, Prof. Jouko Peltonen, Dr. Jixi Zhang, Dr. Igor Vlasov, Dr. Venkata Krishnan, Dr. Digambra Patra, Dr. Tatiana Dolenko, Dr. Tuomas Näreoja, Dr. Markus Peurla, Dr. Sami Koho, Dr. Takahiro Deguchi, Dr. Eudald Casals, Dr. Didem Sen Karaman, Dr. Eva von Haartman, Dr.

Diti Desai, Dr. Anni Määttänen, Tina Gulin, Meraj Hasan Khan, and Lingeshwar Reddy for sharing scientific ideas, research infrastructure and co-operation over the years.

It's my pleasure to thank Dr. Tuomas Näreoja for all the tireless and sincere effort, he has put in mentoring me in research. You have always tried to help me in every possible capacity. Tuomas, you have been an excellent *Guru*, colleague, and a very friendly person. I am enormously thankful to Dr. Sami Koho for playing a vital role in my research as a colleague and co-author. Thanks, Sami, for your ideas, software, and manuscript writing in our CLEM work. I personally owe you big thanks for the *Small* paper. Dr. Markus Peurla is thoroughly thanked for bringing enthusiasm in our CLEM related project. Markus, you have always brought fresh ideas to our projects, and things could not have been possible without your co-operation. You have always been willing to support and welcoming. Dr. Takahiro Deguchi is thanked for facilitating for all those years with microscopes and being a *decent* person around the office corner.

Thanks, Bionanomaterial girls (Diti, Eva, Didem) for being friendly colleagues and providing all kind of nanomaterials needed for my research. I would like this opportunity to especially thank Johan Nyman for providing help during thesis language approval part and continuously cheering up. I am very much thankful to all the colleagues and support staff at Pharmaceutical Sciences Laboratory, Åbo Akademi University, Jari Korhonen from Cell Imaging Core, and Jenni Laine from Electron Microscopy Unit, University of Turku. I am thankful to all current and past members of Bionanomaterials group ÅA and Laboratory of Biophysics, UTU. I wish all the very best for you.

I am very much grateful to Dr. Anita Rozwandowicz-Jansen for all the friendly conversations over the years and keeping the atmosphere very social in our office. My great friends in Turku, Janne Kulpakko and Eudald Casals, you guys are great in every way. It was always pleasured and fun to talk to you on "Our interesting topics". I wish, we remain good friends for a long time to come. My childhood friends back home, Amit, Pawan, and Sarwjeet, I have known you guys for long and thanks for being good friends. I am thankful to Himanshu Kumar, Sangeeta, Ponnuswamy M, Arjun Tiwari, Moin Khan, Meraj Khan, Mukund Sharma, and Farid Siddiqui for friendship.

I am enormously thankful to my parents for providing freedom and unconditional support. I would like this opportunity to thanks my family members and relatives back home, thank you.

Åbo, 2018

Neeraj Prabhakar

References

(1) Cuenca, A. G.; Jiang, H.; Hochwald, S. N.; Delano, M.; Cance, W. G.; Grobmyer, S. R. Emerging Implications of Nanotechnology on Cancer Diagnostics and Therapeutics. *Cancer* **2006**, *107* (3), 459–466.

(2) Ferrari, M. Cancer Nanotechnology: Opportunities and Challenges. *Nat. Rev. Cancer* **2005**, *5* (3), 161–171.

(3) Tanaka, T.; Mangala, L. S.; Vivas-Mejia, P. E.; Nieves-Alicea, R.; Mann, A. P.; Mora, E.; Han, H. D.; Shahzad, M. M. K.; Liu, X.; Bhavane, R.; Gu, J.; Fakhoury, J. R.; Chiappini, C.; Lu, C.; Matsuo, K.; Godin, B.; Stone, R. L.; Nick, A. M.; Lopez-Berestein, G.; Sood, A. K.; Ferrari, M. Sustained Small Interfering RNA Delivery by Mesoporous Silicon Particles. *Cancer Res.* **2010**, *70* (9), 3687–3696.

(4) Rosenholm, J. M.; Meinander, A.; Peuhu, E.; Niemi, R.; Eriksson, J. E.; Sahlgren, C.; Lindén, M. Targeting of Porous Hybrid Silica Nanoparticles to Cancer Cells. *ACS Nano* **2009**, *3* (1), 197–206.

(5) Xu, X.; Ho, W.; Zhang, X.; Bertrand, N.; Farokhzad, O. Cancer Nanomedicine: From Targeted Delivery to Combination Therapy. *Trends Mol. Med.* **2015**, *21* (4), 223–232.

(6) Fundarò, A.; Cavalli, R.; Bargoni, A.; Vighetto, D.; Zara, G. P.; Gasco, M. R. Non-Stealth and Stealth Solid Lipid Nanoparticles (SLN) Carrying Doxorubicin: Pharmacokinetics and Tissue Distribution after I.v. Administration to Rats. *Pharmacol. Res.* **2000**, *42* (4), 337–343.

(7) Meng, H.; Liong, M.; Xia, T.; Li, Z.; Ji, Z.; Zink, J. I.; Nel, A. E. Engineered Design of Mesoporous Silica Nanoparticles to Deliver Doxorubicin and P-Glycoprotein siRNA to Overcome Drug Resistance in a Cancer Cell Line. *ACS Nano* **2010**, *4* (8), 4539–4550.

(8) Steiniger, S. C. J.; Kreuter, J.; Khalansky, A. S.; Skidan, I. N.; Bobruskin, A. I.; Smirnova, Z. S.; Severin, S. E.; Uhl, R.; Kock, M.; Geiger, K. D.; Gelperina, S. E. Chemotherapy of Glioblastoma in Rats Using Doxorubicin-Loaded Nanoparticles. *Int. J. Cancer* **2004**, *109* (5), 759–767.

(9) Wei, H.; Bruns, O. T.; Kaul, M. G.; Hansen, E. C.; Barch, M.; Wiśniowska, A.; Chen, O.; Chen, Y.; Li, N.; Okada, S.; Cordero, J. M.; Heine, M.; Farrar, C. T.; Montana, D. M.; Adam, G.; Ittrich, H.; Jasanoff, A.; Nielsen, P.; Bawendi, M. G. Exceedingly Small Iron Oxide Nanoparticles as Positive MRI Contrast Agents. *Proc. Natl. Acad. Sci. U. S. A.* **2017**, *114* (9), 2325–2330.

(10) Ahmad, M. W.; Xu, W.; Kim, S. J.; Baeck, J. S.; Chang, Y.; Bae, J. E.; Chae, K. S.; Park, J. A.; Kim, T. J.; Lee, G. H. Potential Dual Imaging Nanoparticle: Gd2O3 Nanoparticle. *Sci. Rep.* **2015**, *5* (1), 8549.

(11) Huang, J.; Zhong, X.; Wang, L.; Yang, L.; Mao, H. Improving the Magnetic Resonance Imaging Contrast and Detection Methods with Engineered Magnetic Nanoparticles. *Theranostics* **2012**, *2* (1), 86–102.

(12) Shroff, K.; Kokkoli, E. PEGylated Liposomal Doxorubicin Targeted to ?$_5$?$_1$-Expressing MDA-MB-231 Breast Cancer Cells. *Langmuir* **2012**, *28* (10), 4729–4736.

(13) Park, J. W.; Kirpotin, D. B.; Hong, K.; Shalaby, R.; Shao, Y.; Nielsen, U. B.; Marks, J. D.; Papahadjopoulos, D.; Benz, C. C.; Moore, D.; Papahadjopoulos, D.; Benz, C.; Frigerio, E.; Cassidy, J.; Pike, M.; Ross, M. Tumor Targeting Using Anti-her2 Immunoliposomes. *J. Control. Release* **2001**, *74* (1–3), 95–113.

(14) Symon, Z.; Peyser, A.; Tzemach, D.; Lyass, O.; Sucher, E.; Shezen, E.; Gabizon, A. Selective Delivery of Doxorubicin to Patients with Breast Carcinoma Metastases by Stealth Liposomes. *Cancer* **1999**, *86* (1), 72–78.

(15) Wang, J. Nanoparticle-Based Electrochemical DNA Detection. *Anal. Chim. Acta* **2003**, *500* (1–2), 247–257.

(16) Chung, H. J.; Castro, C. M.; Im, H.; Lee, H.; Weissleder, R. A Magneto-DNA Nanoparticle System for Rapid Detection and Phenotyping of Bacteria. **2013**.

(17) Bregoli, L.; Movia, D.; Gavigan-Imedio, J. D.; Lysaght, J.; Reynolds, J.; Prina-Mello, A. Nanomedicine Applied to Translational Oncology: A Future Perspective on Cancer Treatment. *Nanomedicine Nanotechnology, Biol. Med.* **2016**, *12* (1), 81–103.

(18) Slowing, I. I.; Vivero-Escoto, J. L.; Wu, C.-W.; Lin, V. S.-Y. Mesoporous Silica Nanoparticles as Controlled Release Drug Delivery and Gene Transfection Carriers. *Adv. Drug Deliv. Rev.* **2008**, *60* (11), 1278–1288.

(19) Rosenholm, J. M.; Sahlgren, C.; Lind?n, M. Towards Multifunctional, Targeted Drug Delivery Systems Using Mesoporous Silica Nanoparticles ? Opportunities & Challenges. *Nanoscale* **2010**, *2* (10), 1870.

(20) Haartman, E. von; Jiang, H.; Khomich, A. A.; Zhang, J.; Burikov, S. A.; Dolenko, T. A.; Ruokolainen, J.; Gu, H.; Shenderova, O. A.; Vlasov, I. I.; Rosenholm, J. M. Core–shell Designs of Photoluminescent Nanodiamonds with Porous Silica Coatings for Bioimaging and Drug Delivery I: Fabrication. *J. Mater. Chem. B* **2013**, *1* (18), 2358–2366.

(21) Anselmo, A. C.; Mitragotri, S. Nanoparticles in the Clinic. *Bioeng. Transl. Med.* **2016**, *1* (1), 10–29.

(22) Eifler, A. C.; Thaxton, C. S. Nanoparticle Therapeutics: FDA Approval, Clinical Trials, Regulatory Pathways, and Case Study. In *Methods in molecular biology (Clifton, N.J.)*; 2011; Vol. 726, pp 325–338.

(23) Weissig, V.; Pettinger, T. K.; Murdock, N. Nanopharmaceuticals (Part 1): Products on the Market. *Int. J. Nanomedicine* **2014**, *9*, 4357–4373.

(24) Zugazagoitia, J.; Guedes, C.; Ponce, S.; Ferrer, I.; Molina-Pinelo, S.; Paz-Ares, L. Current Challenges in Cancer Treatment. *Clin. Ther.* **2016**, *38* (7), 1551–1566.

(25) Bhatia, S.; Frangioni, J. V; Hoffman, R. M.; Iafrate, A. J.; Polyak, K. The Challenges Posed by Cancer Heterogeneity. *Nat. Biotechnol.* **2012**, *30* (7), 604–610.

(26) Housman, G.; Byler, S.; Heerboth, S.; Lapinska, K.; Longacre, M.; Snyder, N.; Sarkar, S. Drug Resistance in Cancer: An Overview. *Cancers (Basel).* **2014**, *6* (3), 1769–1792.

(27) Holohan, C.; Van Schaeybroeck, S.; Longley, D. B.; Johnston, P. G. Cancer Drug Resistance: An Evolving Paradigm. *Nat. Rev. Cancer* **2013**, *13* (10), 714–726.

(28) Gottesman, M. M. Mechanisms of Cancer Drug Resistance. *Annu. Rev. Med.* **2002**, *53* (1), 615–627.

(29) Sun, X.; Yu, Q. Intra-Tumor Heterogeneity of Cancer Cells and Its Implications for Cancer Treatment. *Acta Pharmacol. Sin.* **2015**, *36* (10), 1219–1227.

(30) Allison, K. H.; Sledge, G. W. Heterogeneity and Cancer. *Oncology (Williston Park).* **2014**, *28* (9), 772–778.

(31) Alizadeh, A. A.; Aranda, V.; Bardelli, A.; Blanpain, C.; Bock, C.; Borowski, C.; Caldas, C.; Califano, A.; Doherty, M.; Elsner, M.; Esteller, M.; Fitzgerald, R.; Korbel, J. O.; Lichter, P.; Mason, C. E.; Navin, N.; Pe'er, D.; Polyak, K.; Roberts, C. W. M.; Siu, L.; Snyder, A.; Stower, H.; Swanton, C.; Verhaak, R. G. W.; Zenklusen, J. C.; Zuber, J.; Zucman-Rossi, J. Toward Understanding and Exploiting Tumor Heterogeneity. *Nat. Med.* **2015**, *21* (8), 846–853.

(32) Fisher, R.; Pusztai, L.; Swanton, C. Cancer Heterogeneity: Implications for Targeted Therapeutics. *Br. J. Cancer* **2013**, *108* (3), 479–485.

(33) Chin, L.; Andersen, J. N.; Futreal, P. A. Cancer Genomics: From Discovery Science to Personalized Medicine. *Nat. Med.* **2011**, *17* (3), 297–303.

(34) Verma, M. Personalized Medicine and Cancer. *J. Pers. Med.* **2012**, *2* (1), 1–14.

(35) Tabernero, J.; Shapiro, G. I.; LoRusso, P. M.; Cervantes, A.; Schwartz, G. K.; Weiss, G. J.; Paz-Ares, L.; Cho, D. C.; Infante, J. R.; Alsina, M.; Gounder, M. M.; Falzone, R.; Harrop, J.; White, A. C. S.; Toudjarska, I.; Bumcrot, D.; Meyers, R. E.; Hinkle, G.; Svrzikapa, N.; Hutabarat, R. M.; Clausen, V. A.; Cehelsky, J.; Nochur, S. V.; Gamba-Vitalo, C.; Vaishnaw, A. K.; Sah, D. W. Y.; Gollob, J. A.; Burris, H. A. First-in-Humans Trial of an RNA Interference Therapeutic Targeting VEGF and KSP in Cancer Patients with Liver Involvement. *Cancer Discov.* **2013**, *3* (4), 406–417.

(36) Elbashir, S. M.; Lendeckel, W.; Tuschl, T. RNA Interference Is Mediated by 21- and 22-Nucleotide RNAs. *Genes Dev.* **2001**, *15* (2), 188–200.

(37) Fire, A.; Xu, S.; Montgomery, M. K.; Kostas, S. A.; Driver, S. E.; Mello, C. C. Potent and Specific Genetic Interference by Double-Stranded RNA in Caenorhabditis Elegans. *Nature* **1998**, *391* (6669), 806–811.

(38) Gu, S.; Hu, Z.; Ngamcherdtrakul, W.; Castro, D. J.; Morry, J.; Reda, M. M.; Gray, J. W.; Yantasee, W.; Gu, S.; Hu, Z.; Ngamcherdtrakul, W.; Castro, D. J.; Morry, J.; Reda, M. M.; Gray, J. W.; Yantasee, W.; Gu, S.; Hu, Z.; Ngamcherdtrakul, W.; Castro, D. J.; Morry, J.; Reda, M. M.; Gray, J. W.; Yantasee, W. Therapeutic siRNA for Drug-Resistant HER2-Positive Breast Cancer. *Oncotarget* **2016**, *7* (12), 14727–14741.

(39) Wang, Y.-C.; Morrison, G.; Gillihan, R.; Guo, J.; Ward, R. M.; Fu, X.; Botero, M. F.; Healy, N. A.; Hilsenbeck, S. G.; Phillips, G. L.; Chamness, G. C.; Rimawi, M. F.; Osborne, C. K.; Schiff, R. Different Mechanisms for Resistance to Trastuzumab versus Lapatinib in HER2-Positive Breast Cancers--Role of Estrogen Receptor and HER2 Reactivation. *Breast Cancer Res.* **2011**, *13* (6), R121.

(40) Gavrilov, K.; Saltzman, W. M. Therapeutic siRNA: Principles, Challenges, and Strategies. *Yale J. Biol. Med.* **2012**, *85* (2), 187–200.

(41) Borna, H.; Imani, S.; Iman, M.; Azimzadeh Jamalkandi, S. Therapeutic Face of RNAi: *In Vivo* Challenges. *Expert Opin. Biol. Ther.* **2015**, *15* (2), 269–285.

(42) Li, X.; Xie, Q. R.; Zhang, J.; Xia, W.; Gu, H. The Packaging of siRNA within the Mesoporous Structure of Silica Nanoparticles. *Biomaterials* **2011**, *32* (35), 9546–9556.

(43) Na, H.-K.; Kim, M.-H.; Park, K.; Ryoo, S.-R.; Lee, K. E.; Jeon, H.; Ryoo, R.; Hyeon, C.; Min, D.-H. Efficient Functional Delivery of siRNA Using Mesoporous Silica Nanoparticles with Ultralarge Pores. *Small* **2012**, *8* (11), 1752–1761.

(44) Dahlman, J. E.; Barnes, C.; Khan, O. F.; Thiriot, A.; Jhunjunwala, S.; Shaw, T. E.; Xing, Y.; Sager, H. B.; Sahay, G.; Speciner, L.; Bader, A.; Bogorad, R. L.; Yin, H.; Racie, T.; Dong, Y.; Jiang, S.; Seedorf, D.; Dave, A.; Singh Sandhu, K.; Webber, M. J.; Novobrantseva, T.; Ruda, V. M.; Lytton-Jean, A. K. R.; Levins, C. G.; Kalish, B.; Mudge, D. K.; Perez, M.; Abezgauz, L.; Dutta, P.; Smith, L.; Charisse, K.; Kieran, M. W.; Fitzgerald, K.; Nahrendorf, M.; Danino, D.; Tuder, R. M.; von Andrian, U. H.; Akinc, A.; Panigrahy, D.; Schroeder, A.; Koteliansky, V.; Langer, R.; Anderson, D. G. In Vivo Endothelial siRNA Delivery Using Polymeric Nanoparticles with Low Molecular Weight. *Nat. Nanotechnol.* **2014**, *9* (8), 648–655.

(45) Argyo, C.; Weiss, V.; Bräuchle, C.; Bein, T.; Br?uchle, C.; Bein, T. Multifunctional Mesoporous Silica Nanoparticles as a Universal Platform for Drug Delivery - Chemistry of Materials ({ACS} Publications). *Chem. Mater.* **2014**, *26* (1), 435–451.

(46) Lee, H.; Lytton-Jean, A. K. R.; Chen, Y.; Love, K. T.; Park, A. I.; Karagiannis, E. D.; Sehgal, A.; Querbes, W.; Zurenko, C. S.; Jayaraman, M.; Peng, C. G.; Charisse, K.; Borodovsky, A.; Manoharan, M.; Donahoe, J. S.; Truelove, J.; Nahrendorf, M.; Langer, R.; Anderson, D. G. Molecularly Self-Assembled Nucleic Acid Nanoparticles for Targeted in Vivo siRNA Delivery. *Nat. Nanotechnol.* **2012**, *7* (6), 389–393.

(47) Opoku-Damoah, Y.; Wang, R.; Zhou, J.; Ding, Y. Versatile Nanosystem-Based Cancer Theranostics: Design Inspiration and Predetermined Routing. *Theranostics* **2016**, *6* (7), 986–1003.

(48) Bhaskar, S.; Tian, F.; Stoeger, T.; Kreyling, W.; de la Fuente, J. M.; Grazú, V.; Borm, P.; Estrada, G.; Ntziachristos, V.; Razansky, D. Multifunctional Nanocarriers for Diagnostics, Drug Delivery and Targeted Treatment across Blood-Brain Barrier: Perspectives on Tracking and Neuroimaging. *Part. Fibre Toxicol.* **2010**, *7* (1), 3.

(49) Parveen, S.; Misra, R.; Sahoo, S. K. Nanoparticles: A Boon to Drug Delivery, Therapeutics, Diagnostics and Imaging. *Nanomedicine Nanotechnology, Biol. Med.* **2012**, *8* (2), 147–166.

(50) Yigit, M. V.; Moore, A.; Medarova, Z. Magnetic Nanoparticles for Cancer Diagnosis and Therapy. *Pharm. Res.* **2012**, *29* (5), 1180–1188.

(51) Gobbo, O. L.; Sjaastad, K.; Radomski, M. W.; Volkov, Y.; Prina-Mello, A. Magnetic Nanoparticles in Cancer Theranostics. *Theranostics* **2015**, *5* (11), 1249–1263.

(52) Arruebo, M.; Valladares, M.; González-Fernández, África. Antibody-Conjugated Nanoparticles for Biomedical Applications. *J. Nanomater.* **2009**, *2009*, 1–24.

(53) Cardoso, M. M.; Peça, I. N.; Roque, A. C. A. Antibody-Conjugated Nanoparticles for Therapeutic Applications. *Curr. Med. Chem.* **2012**, *19* (19), 3103–3127.

(54) Kim, C.; Galloway, J. F.; Lee, K. H.; Searson, P. C. Universal Antibody Conjugation to Nanoparticles Using the Fc? Receptor I (Fc?RI): Quantitative Profiling Of Membrane Biomarkers. *Bioconjug. Chem.* **2014**, *25* (10), 1893–1901.

(55) Bhunia, S. K.; Saha, A.; Maity, A. R.; Ray, S. C.; Jana, N. R. Carbon Nanoparticle-Based Fluorescent Bioimaging Probes. *Sci. Rep.* **2013**, *3* (1), 1473.

(56) Vlasov, I. I.; Shiryaev, A. A.; Rendler, T.; Steinert, S.; Lee, S.-Y.; Antonov, D.; Vörös, M.; Jelezko, F.; Fisenko, A. V.; Semjonova, L. F.; Biskupek, J.; Kaiser, U.; Lebedev, O. I.; Sildos, I.; Hemmer, P. R.; Konov, V. I.; Gali, A.; Wrachtrup, J. Molecular-Sized Fluorescent Nanodiamonds. *Nat. Nanotechnol.* **2014**, *9* (1), 54–58.

(57) Resch-Genger, U.; Grabolle, M.; Cavaliere-Jaricot, S.; Nitschke, R.; Nann, T. Quantum Dots versus Organic Dyes as Fluorescent Labels. *Nat. Methods* **2008**, *5* (9), 763–775.

(58) Li, J.-L.; Tang, B.; Yuan, B.; Sun, L.; Wang, X.-G. A Review of Optical Imaging and Therapy Using Nanosized Graphene and Graphene Oxide. *Biomaterials* **2013**, *34* (37), 9519–9534.

(59) Reddy, K. L.; Rai, M.; Prabhakar, N.; Arppe, R.; Rai, S. B.; Singh, S. K.; Rosenholm, J. M.; Krishnan, V. Controlled Synthesis, Bioimaging and Toxicity Assessments in Strong Red Emitting Mn 2+ Doped NaYF 4 :Yb 3+ /Ho 3+ Nanophosphors. *RSC Adv.* **2016**, *6* (59), 53698–53704.

(60) Prabhakar, N.; Näreoja, T.; Haartman, E. von; Karaman, D. Ş.; Jiang, H.; Koho, S.; Dolenko, T. A.; Hänninen, P. E.; Vlasov, D. I.; Ralchenko, V. G.; Hosomi, S.; Vlasov, I. I.; Sahlgren, C.; Rosenholm, J. M. Core–shell Designs of Photoluminescent Nanodiamonds with Porous Silica Coatings for Bioimaging and Drug Delivery II: Application. *Nanoscale* **2013**, *5* (9), 3713–3722.

(61) Yue, G.; Su, S.; Li, N.; Shuai, M.; Lai, X.; Astruc, D.; Zhao, P. Gold Nanoparticles as Sensors in the Colorimetric and Fluorescence Detection of Chemical Warfare Agents. *Coord. Chem. Rev.* **2016**, *311*, 75–84.

(62) Bianchini, P.; Peres, C.; Oneto, M.; Galiani, S.; Vicidomini, G.; Diaspro, A. STED Nanoscopy: A Glimpse into the Future. *Cell Tissue Res.* **2015**, *360* (1), 143–150.

(63) Nägerl, U. V.; Willig, K. I.; Hein, B.; Hell, S. W.; Bonhoeffer, T. Live-Cell Imaging of Dendritic Spines by STED Microscopy. *Proc. Natl. Acad. Sci. U. S. A.* **2008**, *105* (48), 18982–18987.

(64) Hell, S. W.; Wichmann, J. Breaking the Diffraction Resolution Limit by Stimulated Emission: Stimulated-Emission-Depletion Fluorescence Microscopy. *Opt. Lett.* **1994**, *19* (11), 780.

(65) Hui, Y. Y.; Cheng, C.-L.; Chang, H.-C. Nanodiamonds for Optical Bioimaging. *J. Phys. D. Appl. Phys.* **2010**, *43* (37), 374021.

(66) Chang, Y.-W.; Chen, S.; Tocheva, E. I.; Treuner-Lange, A.; Löbach, S.; Søgaard-Andersen, L.; Jensen, G. J. Correlated Cryogenic Photoactivated Localization Microscopy and Cryo-Electron Tomography. *Nat. Methods* **2014**, *11* (7), 737–739.

(67) Löschberger, A.; Franke, C.; Krohne, G.; van de Linde, S.; Sauer, M.; Linde, S. van de; Sauer, M.; van de Linde, S.; Sauer, M. Correlative Super-Resolution Fluorescence and Electron

Microscopy of the Nuclear Pore Complex with Molecular Resolution. *J. Cell Sci.* **2014**, *127* (Pt 20), 4351–4355.

(68) Kopek, B. G.; Shtengel, G.; Xu, C. S.; Clayton, D. A.; Hess, H. F. Correlative 3D Superresolution Fluorescence and Electron Microscopy Reveal the Relationship of Mitochondrial Nucleoids to Membranes. *Proc. Natl. Acad. Sci. U. S. A.* **2012**, *109* (16), 6136–6141.

(69) Prasad, V.; Semwogerere, D.; Weeks, E. R. Confocal Microscopy of Colloids. *J. Phys. Condens. Matter* **2007**, *19* (11), 113102.

(70) Zipfel, W. R.; Williams, R. M.; Webb, W. W. Nonlinear Magic: Multiphoton Microscopy in the Biosciences. *Nat. Biotechnol.* **2003**, *21* (11), 1369–1377.

(71) Ustione, A.; Piston, D. W. A Simple Introduction to Multiphoton Microscopy. *J. Microsc.* **2011**, *243* (3), 221–226.

(72) Levene, M. J.; Dombeck, D. A.; Kasischke, K. A.; Molloy, R. P.; Webb, W. W. In Vivo Multiphoton Microscopy of Deep Brain Tissue. *J. Neurophysiol.* **2004**, *91* (4), 1908–1912.

(73) Svoboda, K.; Yasuda, R. Primer Principles of Two-Photon Excitation Microscopy and Its Applications to Neuroscience. *Neuron* **2006**, *50*, 823–839.

(74) Klar, T. A.; Jakobs, S.; Dyba, M.; Egner, A.; Hell, S. W. Fluorescence Microscopy with Diffraction Resolution Barrier Broken by Stimulated Emission. *Proc. Natl. Acad. Sci. U. S. A.* **2000**, *97* (15), 8206–8210.

(75) Hell, S. W.; Wichmann, J. Stimulated-Emission-Depletion Fluorescence Microscopy. *Opt. Lett.* **1994**, *19* (11), 780–782.

(76) Arroyo-Camejo, S.; Adam, M.-P.; Besbes, M.; Hugonin, J.-P.; Jacques, V.; Greffet, J.-J.; Roch, J.-F.; Hell, S. W.; Treussart, F. Stimulated Emission Depletion Microscopy Resolves Individual Nitrogen Vacancy Centers in Diamond Nanocrystals. *ACS Nano* **2013**, *7* (12), 10912–10919.

(77) Gustafsson, M. G. L. Nonlinear Structured-Illumination Microscopy: Wide-Field Fluorescence Imaging with Theoretically Unlimited Resolution. *Proc. Natl. Acad. Sci. U. S. A.* **2005**, *102* (37), 13081–13086.

(78) Gustafsson, M. G. L. Surpassing the Lateral Resolution Limit by a Factor of Two Using Structured Illumination Microscopy. *J. Microsc.* **2000**, *198* (2), 82–87.

(79) Betzig, E.; Patterson, G. H.; Sougrat, R.; Lindwasser, O. W.; Olenych, S.; Bonifacino, J. S.; Davidson, M. W.; Lippincott-Schwartz, J.; Hess, H. F. Imaging Intracellular Fluorescent Proteins at Nanometer Resolution. *Science* **2006**, *313* (5793), 1642–1645.

(80) Shroff, H.; Galbraith, C. G.; Galbraith, J. A.; Betzig, E. Live-Cell Photoactivated Localization Microscopy of Nanoscale Adhesion Dynamics. *Nat. Methods* **2008**, *5* (5), 417–423.

(81) Huang, B.; Bates, M.; Zhuang, X. Super-Resolution Fluorescence Microscopy. *Annu. Rev. Biochem.* **2009**, *78*, 993–1016.

(82) Willig, K. I.; Rizzoli, S. O.; Westphal, V.; Jahn, R.; Hell, S. W. {STED} Microscopy Reveals That Synaptotagmin Remains Clustered after Synaptic Vesicle Exocytosis. *Nature* **2006**, *440* (7086), 935–939.

(83) Eggeling, C.; Willig, K. I.; Barrantes, F. J. STED Microscopy of Living Cells - New Frontiers in Membrane and Neurobiology. *J. Neurochem.* **2013**, *126* (2), 203–212.

(84) Mishina, N. M.; Mishin, A. S.; Belyaev, Y.; Bogdanova, E. A.; Lukyanov, S.; Schultz, C.; Belousov, V. V. Live-Cell STED Microscopy with Genetically Encoded Biosensor. *Nano Lett.* **2015**, *15* (5), 2928–2932.

(85) Laporte, G.; Psaltis, D. STED Imaging of Green Fluorescent Nanodiamonds Containing Nitrogen-Vacancy-Nitrogen Centers. *Biomed. Opt. Express* **2015**, *7* (1), 34–44.

(86) Chalfie, M. GFP: Lighting up Life. *Proc. Natl. Acad. Sci. U. S. A.* **2009**, *106* (25), 10073–10080.

(87) Lichtman, J. W.; Conchello, J.-A. Fluorescence Microscopy. *Nat. Methods* **2005**, *2* (12), 910–919.

(88) Kwok, S. J. J.; Choi, M.; Bhayana, B.; Zhang, X.; Ran, C.; Yun, S.-H. Two-Photon Excited Photoconversion of Cyanine-Based Dyes. *Nat. Publ. Gr.* **2016**.

(89) Lau, L.; Lee, Y. L.; Matis, M.; Axelrod, J.; Stearns, T.; Moerner, W. E. STED Super-Resolution Microscopy in Drosophila Tissue and in Mammalian Cells. *Proc. SPIE--the Int. Soc. Opt. Eng.* **2011**, *7910*.

(90) Beater, S.; Holzmeister, P.; Pibiri, E.; Lalkens, B.; Tinnefeld, P. Choosing Dyes for Cw-STED Nanoscopy Using Self-Assembled Nanorulers. *Phys. Chem. Chem. Phys.* **2014**, *16* (15), 6990–6996.

(91) Zheng, Q.; Jockusch, S.; Zhou, Z.; Blanchard, S. C. The Contribution of Reactive Oxygen Species to the Photobleaching of Organic Fluorophores. *Photochem. Photobiol.* **2014**, *90* (2), 448–454.

(92) Chen, G.; Roy, I.; Yang, C.; Prasad, P. N. Nanochemistry and Nanomedicine for Nanoparticle-Based Diagnostics and Therapy. *Chem. Rev.* **2016**, *116* (5), 2826–2885.

(93) Baetke, S. C.; Lammers, T.; Kiessling, F. Applications of Nanoparticles for Diagnosis and Therapy of Cancer. *Br. J. Radiol.* **2015**, *88* (1054), 20150207.

(94) de la Rica, R.; Aili, D.; Stevens, M. M. Enzyme-Responsive Nanoparticles for Drug Release and Diagnostics. *Adv. Drug Deliv. Rev.* **2012**, *64* (11), 967–978.

(95) Lin, J.; Chen, X.; Huang, P. Graphene-Based Nanomaterials for Bioimaging. *Adv. Drug Deliv. Rev.* **2016**, *105*, 242–254.

(96) Puzyr, A. P.; Baron, A. V.; Purtov, K. V.; Bortnikov, E. V.; Skobelev, N. N.; Mogilnaya, O. A.; Bondar, V. S. Nanodiamonds with Novel Properties: A Biological Study. *Diam. Relat. Mater.* **2007**, *16* (12), 2124–2128.

(97) Zwicke, G. L.; Mansoori, G. A.; Jeffery, C. J. Utilizing the Folate Receptor for Active Targeting of Cancer Nanotherapeutics. *Nano Rev.* **2012**, *3*.

(98) Rosenholm, J. M.; Peuhu, E.; Eriksson, J. E.; Sahlgren, C.; Lindén, M. Targeted Intracellular Delivery of Hydrophobic Agents Using Mesoporous Hybrid Silica Nanoparticles as Carrier Systems. *Nano Lett.* **2009**, *9* (9), 3308–3311.

(99) Liu, X.; Wang, Y.; Hnatowich, D. J. A Nanoparticle for Tumor Targeted Delivery of Oligomers. In *Methods in molecular biology (Clifton, N.J.)*; 2011; Vol. 764, pp 91–105.

(100) Wolfbeis, O. S.; Zhou, J. C.; Xiao, J. W.; Wang, Y. F.; Sun, L. D.; Yan, C. H.; Ma, Y.; Cai, L.; Peng, W.; Xiao, Q.; Ni, D.; Liu, J.; Shi, J.; Hartley, R. C.; Smith, R. A. J.; Krieg, T.; Brookes, P. S.; Murphy, M. P. An Overview of Nanoparticles Commonly Used in Fluorescent Bioimaging. *Chem. Soc. Rev.* **2015**, *44* (14), 4743–4768.

(101) Tran, H. N.; Lien Nghiem, T. H.; Duong Vu, T. T.; Pham, M. T.; Nguyen, T. Van; Tran, T. T.; Chu, V. H.; Tong, K. T.; Tran, T. T.; Xuan Le, T. T.; Brochon, J.-C.; Nguyen, T. Q.; Hoang, M. N.; Duong, C. N.; Nguyen, T. T.; Hoang, A. T.; Nguyen, P. H. Dye-Doped Silica-Based Nanoparticles for Bioapplications. *Adv. Nat. Sci. Nanosci. Nanotechnol.* **2013**, *4* (4), 43001.

(102) Tenuta, T.; Monopoli, M. P.; Kim, J.; Salvati, A.; Dawson, K. A.; Sandin, P.; Lynch, I. Elution of Labile Fluorescent Dye from Nanoparticles during Biological Use. *PLoS One* **2011**, *6* (10), e25556.

(103) Wu, S.-H.; Lin, Y.-S.; Hung, Y.; Chou, Y.-H.; Hsu, Y.-H.; Chang, C.; Mou, C.-Y. Multifunctional Mesoporous Silica Nanoparticles for Intracellular Labeling and Animal Magnetic Resonance Imaging Studies. *ChemBioChem* **2008**, *9* (1), 53–57.

(104) Saha, K.; Agasti, S. S.; Kim, C.; Li, X.; Rotello, V. M. Gold Nanoparticles in Chemical and Biological Sensing. *Chem. Rev.* **2012**, *112* (5), 2739–2779.

(105) Chen, D.; Dougherty, C. A.; Zhu, K.; Hong, H. Theranostic Applications of Carbon Nanomaterials in Cancer: Focus on Imaging and Cargo Delivery. *J. Control. Release* **2015**, *210*, 230–245.

(106) Nguyen, P.-D.; Son, S. J.; Min, J. Upconversion Nanoparticles in Bioassays, Optical Imaging and Therapy. *J. Nanosci. Nanotechnol.* **2014**, *14* (1), 157–174.

(107) Wang, M.; Abbineni, G.; Clevenger, A.; Mao, C.; Xu, S. Upconversion Nanoparticles: Synthesis, Surface Modification and Biological Applications. *Nanomedicine Nanotechnology, Biol. Med.* **2011**, *7* (6), 710–729.

(108) Amoroso, A. J.; Pope, S. J. A. Using Lanthanide Ions in Molecular Bioimaging. *Chem. Soc. Rev.* **2015**, *44* (14), 4723–4742.

(109) Heffern, M. C.; Matosziuk, L. M.; Meade, T. J. Lanthanide Probes for Bioresponsive Imaging. *Chem. Rev.* **2014**, *114* (8), 4496–4539.

(110) Friedman, R. Nano Dot Technology Enters Clinical Trials. *JNCI J. Natl. Cancer Inst.* **2011**, *103* (19), 1428–1429.

(111) Li, Z.; Barnes, J. C.; Bosoy, A.; Stoddart, J. F.; Zink, J. I. Mesoporous Silica Nanoparticles in Biomedical Applications. *Chem. Soc. Rev.* **2012**, *41* (7), 2590.

(112) Zhang, J.; Prabhakar, N.; Näreoja, T.; Rosenholm, J. M. Semiconducting Polymer Encapsulated Mesoporous Silica Particles with Conjugated Europium Complexes: Toward

Enhanced Luminescence under Aqueous Conditions. *ACS Appl. Mater. Interfaces* **2014**, *6* (21).

(113) Zhang, D.; Wang, X.; Qiao, Z.; Tang, D.; Liu, Y.; Huo, Q. Synthesis and Characterization of Novel Lanthanide(III) Complexes-Functionalized Mesoporous Silica Nanoparticles as Fluorescent Nanomaterials. *J. Phys. Chem. C* **2010**, *114* (29), 12505–12510.

(114) Yuan, N.; Liang, Y.; Erichsen, E. S.; Anwander, R. Lanthanide Complex-Incorporated Periodic Mesoporous Organosilica Nanospheres with Tunable Photoluminescence. *RSC Adv.* **2015**, *5* (101), 83368–83376.

(115) Desai, D.; Karaman, D. Sen; Prabhakar, N.; Tadayon, S.; Duchanoy, A.; Toivola, D. M.; Rajput, S.; Näreoja, T.; Rosenholm, J. M.; Diti Desai, D. S. K.; Desai, D.; Karaman, D. Sen; Prabhakar, N.; Tadayon, S.; Duchanoy, A.; Toivola, D. M.; Rajput, S.; N?reoja, T.; Rosenholm, J. M. Design Considerations for Mesoporous Silica Nanoparticulate Systems in Facilitating Biomedical Applications. *Mesoporous Biomater.* **2014**, *1* (1), 16–43.

(116) Ruedas-Rama, M. J.; Walters, J. D.; Orte, A.; Hall, E. A. H. Fluorescent Nanoparticles for Intracellular Sensing: A Review. *Anal. Chim. Acta* **2012**, *751*, 1–23.

(117) Schrand, A. M.; Hens, S. A. C.; Shenderova, O. A. Nanodiamond Particles: Properties and Perspectives for Bioapplications. *Crit. Rev. Solid State Mater. Sci.* **2009**, *34* (1), 18–74.

(118) Hong, G.; Diao, S.; Antaris, A. L.; Dai, H. Carbon Nanomaterials for Biological Imaging and Nanomedicinal Therapy. *Chem. Rev.* **2015**, *115* (19), 10816–10906.

(119) Vaijayanthimala, V.; Tzeng, Y.-K.; Chang, H.-C.; Li, C.-L. The Biocompatibility of Fluorescent Nanodiamonds and Their Mechanism of Cellular Uptake. *Nanotechnology* **2009**, *20* (42), 425103.

(120) Sun, X.; Liu, Z.; Welsher, K.; Robinson, J. T.; Goodwin, A.; Zaric, S.; Dai, H. Nano-Graphene Oxide for Cellular Imaging and Drug Delivery. *Nano Res.* **2008**, *1* (3), 203–212.

(121) Kumar Bhunia, S.; Saha, A.; Maity, A. R.; Ray, S. C.; Jana, N. R.; Bhunia, S. K.; Saha, A.; Maity, A. R.; Ray, S. C.; Jana, N. R. Carbon Nanoparticle-Based Fluorescent Bioimaging Probes. *3*.

(122) Ciftan Hens, S.; Lawrence, W. G.; Kumbhar, A. S.; Shenderova, O. Photoluminescent Nanostructures from Graphite Oxidation. *J. Phys. Chem. C* **2012**, *116* (37), 20015–20022.

(123) Prabhakar, N.; Näreoja, T.; von Haartman, E.; Şen Karaman, D.; Burikov, S. A.; Dolenko, T. A.; Deguchi, T.; Mamaeva, V.; Hänninen, P. E.; Vlasov, I. I.; Shenderova, O. A.; Rosenholm, J. M. Functionalization of Graphene Oxide Nanostructures Improves Photoluminescence and Facilitates Their Use as Optical Probes in Preclinical Imaging. *Nanoscale* **2015**, *7* (23), 10410–10420.

(124) Su, L.-J.; Fang, C.-Y.; Chang, Y.-T.; Chen, K.-M.; Yu, Y.-C.; Hsu, J.-H.; Chang, H.-C. Creation of High Density Ensembles of Nitrogen-Vacancy Centers in Nitrogen-Rich Type Ib Nanodiamonds. *Nanotechnology* **2013**, *24* (31), 315702.

(125) Doherty, M. W.; Manson, N. B.; Delaney, P.; Jelezko, F.; Wrachtrup, J.; Hollenberg, L. C. L. The Nitrogen-Vacancy Colour Centre in Diamond. *Phys. Rep.* **2013**, *528* (1), 1–45.

(126) Budker, D. Diamond Nanosensors: The Sense of Colour Centres. *Nat. Phys.* **2011**, *7* (6), 453–454.

(127) de Boer, P.; Hoogenboom, J. P.; Giepmans, B. N. G. Correlated Light and Electron Microscopy: Ultrastructure Lights Up! *Nat. Methods* **2015**, *12* (6), 503–513.

(128) Takizawa, T.; Suzuki, K.; Robinson, J. M. Correlative Microscopy Using FluoroNanogold on Ultrathin Cryosections: Proof of Principle. *J. Histochem. Cytochem.* **1998**, *46* (10), 1097–1102.

(129) Wu, C.; He, Q.; Zhu, A.; Yang, H.; Liu, Y. Probing the Protein Conformation and Adsorption Behaviors in Nanographene Oxide-Protein Complexes. *J. Nanosci. Nanotechnol.* **2014**, *14* (3), 2591–2598.

(130) Li, J.; Zhang, W.; Chung, T.-F.; Slipchenko, M. N.; Chen, Y. P.; Cheng, J.-X.; Yang, C. Highly Sensitive Transient Absorption Imaging of Graphene and Graphene Oxide in Living Cells and Circulating Blood. *Sci. Rep.* **2015**, *5* (1), 12394.

(131) Zhang, X.; Wang, S.; Liu, M.; Yang, B.; Feng, L.; Ji, Y.; Tao, L.; Wei, Y.; Yamamoto, K.; Hu, R.; Gao, H.; Wei, H.; Zhang, H.; Sun, H.; Yang, B. Size Tunable Fluorescent Nano-Graphite Oxides: Preparation and Cell Imaging Applications. *Phys. Chem. Chem. Phys.* **2013**, *15* (43), 19013.

(132) Fröhlich, E. The Role of Surface Charge in Cellular Uptake and Cytotoxicity of Medical Nanoparticles. *Int. J. Nanomedicine* **2012**, *7*, 5577–5591.

(133) Verma, A.; Stellacci, F. Effect of Surface Properties on Nanoparticle???Cell Interactions. *Small* **2010**, *6* (1), 12–21.

(134) Şen Karaman, D.; Gulin-Sarfraz, T.; Hedström, G.; Duchanoy, A.; Eklund, P.; Rosenholm, J. M. Rational Evaluation of the Utilization of PEG-PEI Copolymers for the Facilitation of Silica Nanoparticulate Systems in Biomedical Applications. *J. Colloid Interface Sci.* **2014**, *418*, 300–310.

(135) Alexis, F.; Zeng, J.; Shu, W. PEI Nanoparticles for Targeted Gene Delivery. *CSH Protoc.* **2006**, *2006* (1), pdb.prot4451.

(136) Mout, R.; Moyano, D. F.; Rana, S.; Rotello, V. M. Surface Functionalization of Nanoparticles for Nanomedicine. *Chem. Soc. Rev.* **2012**, *41* (7), 2539–2544.

(137) Mamaeva, V.; Rosenholm, J. M.; Bate-Eya, L. T.; Bergman, L.; Peuhu, E.; Duchanoy, A.; Fortelius, L. E.; Landor, S.; Toivola, D. M.; Lindén, M.; Sahlgren, C. Mesoporous Silica Nanoparticles as Drug Delivery Systems for Targeted Inhibition of Notch Signaling in Cancer. *Mol. Ther.* **2011**, *19* (8), 1538–1546.

(138) Buchman, Y. K.; Lellouche, E.; Zigdon, S.; Bechor, M.; Michaeli, S.; Lellouche, J.-P. Silica Nanoparticles and Polyethyleneimine (PEI)-Mediated Functionalization: A New Method of PEI Covalent Attachment for siRNA Delivery Applications. *Bioconjug. Chem.* **2013**, *24* (12), 2076–2087.

(139) Lutz, G. J.; Sirsi, S. R.; Williams, J. H. {PEG}-{PEI} Copolymers for Oligonucleotide Delivery to Cells and Tissues. *Methods Mol. Biol.* **2008**, *433*, 141–158.

(140) Sakurai, Y.; Hatakeyama, H.; Sato, Y.; Akita, H.; Takayama, K.; Kobayashi, S.; Futaki, S.; Harashima, H. Endosomal Escape and the Knockdown Efficiency of Liposomal-siRNA by the Fusogenic Peptide shGALA. *Biomaterials* **2011**, *32* (24), 5733–5742.

(141) Dominska, M.; Dykxhoorn, D. M. Breaking down the Barriers: siRNA Delivery and Endosome Escape. *J. Cell Sci.* **2010**.

(142) Ruoslahti, E. Peptides as Targeting Elements and Tissue Penetration Devices for Nanoparticles. *Adv. Mater.* **2012**, *24* (28), 3747–3756.

(143) El-Sayed, A.; Futaki, S.; Harashima, H. Delivery of Macromolecules Using Arginine-Rich Cell-Penetrating Peptides: Ways to Overcome Endosomal Entrapment. *AAPS J.* **2009**, *11* (1), 13–22.

(144) ELSAYED, I.; HUANG, X.; ELSAYED, M. Selective Laser Photo-Thermal Therapy of Epithelial Carcinoma Using Anti-EGFR Antibody Conjugated Gold Nanoparticles. *Cancer Lett.* **2006**, *239* (1), 129–135.

(145) Schiffelers, R. M. Cancer siRNA Therapy by Tumor Selective Delivery with Ligand-Targeted Sterically Stabilized Nanoparticle. *Nucleic Acids Res.* **2004**, *32* (19), e149–e149.

(146) Rosenholm, J. M.; Mamaeva, V.; Sahlgren, C.; Lind?n, M. Nanoparticles in Targeted Cancer Therapy: Mesoporous Silica Nanoparticles Entering Preclinical Development Stage. *Nanomedicine* **2012**, *7* (1), 111–120.

(147) Rosenholm, J.; Sahlgren, C.; Lind?n, M.; Mergny, M. D.; Scherman, D.; Demeneix, B.; Behr, J.-P.; Chen, Y.; Huang, D.-M.; Yang, C.-S.; Mou, C.-Y.; Chen, Y.-C.; Durand, J. O. Cancer-Cell Targeting and Cell-Specific Delivery by Mesoporous Silica Nanoparticles. *J. Mater. Chem.* **2010**, *20* (14), 2707.

(148) Werner, M. E.; Karve, S.; Sukumar, R.; Cummings, N. D.; Copp, J. A.; Chen, R. C.; Zhang, T.; Wang, A. Z. Folate-Targeted Nanoparticle Delivery of Chemo- and Radiotherapeutics for the Treatment of Ovarian Cancer Peritoneal Metastasis. *Biomaterials* **2011**, *32* (33), 8548–8554.

(149) Kularatne, S. A.; Low, P. S. Targeting of Nanoparticles: Folate Receptor. In *Methods in molecular biology (Clifton, N.J.)*; 2010; Vol. 624, pp 249–265.

(150) Daniels, T. R.; Bernabeu, E.; Rodríguez, J. A.; Patel, S.; Kozman, M.; Chiappetta, D. A.; Holler, E.; Ljubimova, J. Y.; Helguera, G.; Penichet, M. L. The Transferrin Receptor and the Targeted Delivery of Therapeutic Agents against Cancer. *Biochim. Biophys. Acta* **2012**, *1820* (3), 291–317.

(151) Nag, M.; Gajbhiye, V.; Kesharwani, P.; Jain, N. K. Transferrin Functionalized Chitosan-PEG Nanoparticles for Targeted Delivery of Paclitaxel to Cancer Cells. *Colloids Surfaces B Biointerfaces* **2016**, *148*, 363–370.

(152) Gao, X.; Tao, W.; Lu, W.; Zhang, Q.; Zhang, Y.; Jiang, X.; Fu, S. Lectin-Conjugated PEG?PLA Nanoparticles: Preparation and Brain Delivery after Intranasal Administration. *Biomaterials* **2006**, *27* (18), 3482–3490.

(153) Singh, A.; Dilnawaz, F.; Sahoo, S. K.; Valette, A.; Swirsky, D. Long Circulating Lectin Conjugated Paclitaxel Loaded Magnetic Nanoparticles: A New Theranostic Avenue for Leukemia Therapy. *PLoS One* **2011**, *6* (11), e26803.

(154) Byrne, J. D.; Betancourt, T.; Brannon-Peppas, L. Active Targeting Schemes for Nanoparticle Systems in Cancer Therapeutics. *Adv. Drug Deliv. Rev.* **2008**, *60* (15), 1615–1626.

(155) Bazak, R.; Houri, M.; El Achy, S.; Kamel, S.; Refaat, T. Cancer Active Targeting by Nanoparticles: A Comprehensive Review of Literature. *J. Cancer Res. Clin. Oncol.* **2015**, *141* (5), 769–784.

(156) Bertrand, N.; Wu, J.; Xu, X.; Kamaly, N.; Farokhzad, O. C. Cancer Nanotechnology: The Impact of Passive and Active Targeting in the Era of Modern Cancer Biology. *Adv. Drug Deliv. Rev.* **2014**, *66*, 2–25.

(157) Maeda, H. The Enhanced Permeability and Retention (EPR) Effect in Tumor Vasculature: The Key Role of Tumor-Selective Macromolecular Drug Targeting. *Adv. Enzyme Regul.* **2001**, *41*, 189–207.

(158) Maeda, H.; Wu, J.; Sawa, T.; Matsumura, Y.; Hori, K. Tumor Vascular Permeability and the EPR Effect in Macromolecular Therapeutics: A Review. *J. Control. Release* **2000**, *65* (1–2), 271–284.

(159) Jokerst, J. V; Lobovkina, T.; Zare, R. N.; Gambhir, S. S. Nanoparticle PEGylation for Imaging and Therapy. *Nanomedicine (Lond).* **2011**, *6* (4), 715–728.

(160) Li, S.-D.; Huang, L. Stealth Nanoparticles: High Density but Sheddable PEG Is a Key for Tumor Targeting. *J. Control. Release* **2010**, *145* (3), 178–181.

(161) Gref, R.; Lck, M.; Quellec, P.; Marchand, M.; Dellacherie, E.; Harnisch, S.; Blunk, T.; M?ller, R. . ?Stealth? Corona-Core Nanoparticles Surface Modified by Polyethylene Glycol (PEG): Influences of the Corona (PEG Chain Length and Surface Density) and of the Core Composition on Phagocytic Uptake and Plasma Protein Adsorption. *Colloids Surfaces B Biointerfaces* **2000**, *18* (3–4), 301–313.

(162) Boussif, O.; Lezoualc'h, F.; Zanta, M. A.; Mergny, M. D.; Scherman, D.; Demeneix, B.; Behr, J. P. A Versatile Vector for Gene and Oligonucleotide Transfer into Cells in Culture and in Vivo: Polyethylenimine. *Proc. Natl. Acad. Sci. U. S. A.* **1995**, *92* (16), 7297–7301.

(163) Lungwitz, U.; Breunig, M.; Blunk, T.; G?pferich, A.; Göpferich, A. Polyethylenimine-Based Non-Viral Gene Delivery Systems. *Eur. J. Pharm. Biopharm.* **2005**, *60* (2), 247–266.

(164) Lee, S.-Y.; Huh, M. S.; Lee, S.; Lee, S. J.; Chung, H.; Park, J. H.; Oh, Y.-K.; Choi, K.; Kim, K.; Kwon, I. C. Stability and Cellular Uptake of Polymerized siRNA (Poly-siRNA)/polyethylenimine (PEI) Complexes for Efficient Gene Silencing. *J. Control. Release* **2010**, *141* (3), 339–346.

(165) Roiter, Y.; Ornatska, M.; Rammohan, A. R.; Balakrishnan, J.; Heine, D. R.; Minko, S. Interaction of Nanoparticles with Lipid Membrane. *Nano Lett.* **2008**, *8* (3), 941–944.

(166) Elbashir, S. M.; Harborth, J.; Lendeckel, W.; Yalcin, A.; Weber, K.; Tuschl, T. Duplexes of 21-Nucleotide RNAs Mediate RNA Interference in Cultured Mammalian Cells. *Nature* **2001**, *411* (6836), 494–498.

(167) Carthew, R. W.; Sontheimer, E. J. Origins and Mechanisms of miRNAs and siRNAs. *Cell* **2009**, *136* (4), 642–655.

(168) Miele, E.; Spinelli, G. P.; Miele, E.; Fabrizio, E. Di; Ferretti, E.; Tomao, S.; Gulino, A. Nanoparticle-Based Delivery of Small Interfering RNA: Challenges for Cancer Therapy. *Int. J. Nanomedicine* **2012**, *7*, 3637–3657.

(169) Aagaard, L.; Rossi, J. J. RNAi Therapeutics: Principles, Prospects and Challenges. *Adv. Drug Deliv. Rev.* **2007**, *59* (2–3), 75–86.

(170) Chen, M.; Du, Q.; Zhang, H.-Y.; Wahlestedt, C.; Liang, Z. Vector-Based siRNA Delivery Strategies for High-Throughput Screening of Novel Target Genes. *J. RNAi Gene Silencing* **2005**, *1* (1), 5–11.

(171) Urban-Klein, B.; Werth, S.; Abuharbeid, S.; Czubayko, F.; Aigner, A. RNAi-Mediated Gene-Targeting through Systemic Application of Polyethylenimine (PEI)-Complexed siRNA in Vivo. *Gene Ther.* **2005**, *12* (5), 461–466.

(172) Buyens, K.; De Smedt, S. C.; Braeckmans, K.; Demeester, J.; Peeters, L.; van Grunsven, L. A.; de Mollerat du Jeu, X.; Sawant, R.; Torchilin, V.; Farkasova, K.; Ogris, M.; Sanders, N. N. Liposome Based Systems for Systemic siRNA Delivery: Stability in Blood Sets the Requirements for Optimal Carrier Design. *J. Control. Release* **2012**, *158* (3), 362–370.

(173) Hom, C.; Lu, J.; Liong, M.; Luo, H.; Li, Z.; Zink, J. I.; Tamanoi, F. Mesoporous Silica Nanoparticles Facilitate Delivery of {siRNA} to Shutdown Signaling Pathways in Mammalian Cells. *Small* **2010**, *6* (11), 1185–1190.

(174) Li, X.; Chen, Y.; Wang, M.; Ma, Y.; Xia, W.; Gu, H. A Mesoporous Silica Nanoparticle - PEI - Fusogenic Peptide System for siRNA Delivery in Cancer Therapy. *Biomaterials* **2013**, *34* (4), 1391–1401.

(175) Prabhakar, N.; Zhang, J.; Desai, D.; Casals, E.; Gulin-Sarfraz, T.; Näreoja, T.; Westermarck, J.; Rosenholm, J. M. J. M. Stimuli-Responsive Hybrid Nanocarriers Developed by Controllable Integration of Hyperbranched PEI with Mesoporous Silica Nanoparticles for Sustained Intracellular siRNA Delivery. *Int. J. Nanomedicine* **2016**, *11*, 6591–6608.

(176) Möller, K.; Müller, K.; Engelke, H.; Bräuchle, C.; Wagner, E.; Bein, T. Highly Efficient siRNA Delivery from Core–shell Mesoporous Silica Nanoparticles with Multifunctional Polymer Caps. *Nanoscale* **2016**, *8* (7), 4007–4019.

(177) Finlay, J.; Roberts, C. M.; Dong, J.; Zink, J. I.; Tamanoi, F.; Glackin, C. A. Mesoporous Silica Nanoparticle Delivery of Chemically Modified siRNA against TWIST1 Leads to Reduced Tumor Burden. *Nanomedicine Nanotechnology, Biol. Med.* **2015**, *11* (7), 1657–1666.

(178) Mamaeva, V.; Sahlgren, C.; Lindén, M. Mesoporous Silica Nanoparticles in Medicine-Recent Advances. *Adv. Drug Deliv. Rev.* **2013**, *65* (5), 689–702.

(179) M. Rosenholm, J.; Sahlgren, C.; Linden, M. Multifunctional Mesoporous Silica Nanoparticles for Combined Therapeutic, Diagnostic and Targeted Action in Cancer Treatment. *Curr. Drug Targets* **2011**, *12* (8), 1166–1186.

(180) Rosenholm, J. M.; Lindén, M. Wet-Chemical Analysis of Surface Concentration of Accessible Groups on Different Amino-Functionalized Mesoporous SBA-15 Silicas. *Chem. Mater.* **2007**, *19* (20), 5023–5034.

(181) Hartono, S. B.; Yu, M.; Gu, W.; Yang, J.; Strounina, E.; Wang, X.; Qiao, S.; Yu, C.; Shizhang Qiao; Yu, C. Synthesis of Multi-Functional Large Pore Mesoporous Silica Nanoparticles as Gene Carriers. *Nanotechnology* **2014**, *25* (5), 55701.

(182) Lokman, N. A.; Elder, A. S. F.; Ricciardelli, C.; Oehler, M. K. Chick Chorioallantoic Membrane (CAM) Assay as an In Vivo Model to Study the Effect of Newly Identified Molecules on Ovarian Cancer Invasion and Metastasis. *Int. J. Mol. Sci.* **2012**, *13* (8), 9959–9970.

(183) Koho, S.; Deguchi, T.; Hänninen, P. E. A Software Tool for Tomographic Axial Superresolution in STED Microscopy. *J. Microsc.* **2015**, *260* (2), 208–218.

(184) Schrand, A. M.; Hens, S. A. C.; Shenderova, O. A. Nanodiamond Particles: Properties and Perspectives for Bioapplications. *Crit. Rev. Solid State Mater. Sci.* **2009**, *34* (1–2), 18–74.

(185) Chang, Y.-R.; Lee, H.-Y.; Chen, K.; Chang, C.-C.; Tsai, D.-S.; Fu, C.-C.; Lim, T.-S.; Tzeng, Y.-K.; Fang, C.-Y.; Han, C.-C.; Chang, H.-C.; Fann, W. Mass Production and Dynamic Imaging of Fluorescent Nanodiamonds. *Nat. Nanotechnol.* **2008**, *3* (5), 284–288.

(186) Liu, K.-K.; Wang, C.-C.; Cheng, C.-L.; Chao, J.-I. Endocytic Carboxylated Nanodiamond for the Labeling and Tracking of Cell Division and Differentiation in Cancer and Stem Cells. *Biomaterials* **2009**, *30* (26), 4249–4259.

(187) Liu, K.-K.; Cheng, C.-L.; Chang, C.-C.; Chao, J.-I. Biocompatible and Detectable Carboxylated Nanodiamond on Human Cell. *Nanotechnology* **2007**, *18* (32), 325102.

(188) Doherty, G. J.; McMahon, H. T. Mechanisms of Endocytosis. *Annu. Rev. Biochem.* **2009**, *78* (1), 857–902.

(189) Padman, B. S.; Bach, M.; Ramm, G. An Improved Procedure for Subcellular Spatial Alignment during Live-Cell CLEM. *PLoS One* **2014**, *9* (4).

(190) de Boer, P.; Hoogenboom, J. P.; Giepmans, B. N. G. Correlated Light and Electron Microscopy: Ultrastructure Lights Up! *Nat. Methods* **2015**, *12* (6), 503–513.

(191) Mironov, A. A.; Beznoussenko, G. V. Correlative Light-Electron Microscopy: A Potent Tool for the Imaging of Rare or Unique Cellular and Tissue Events and Structures. *Methods Enzymol.* **2012**, *504* (3), 201–219.

(192) Sun, X.; Liu, Z.; Welsher, K.; Robinson, J. T.; Goodwin, A.; Zaric, S.; Dai, H. Nano-Graphene Oxide for Cellular Imaging and Drug Delivery. *Nano Res.* **2008**, *1* (3), 203–212.

(193) Feng, L.; Yang, X.; Shi, X.; Tan, X.; Peng, R.; Wang, J.; Liu, Z. Polyethylene Glycol and Polyethylenimine Dual-Functionalized Nano-Graphene Oxide for Photothermally Enhanced Gene Delivery. *Small* **2013**, *9* (11), 1989–1997.

(194) Lutz, G. J.; Sirsi, S. R.; Williams, J. H. PEG-PEI Copolymers for Oligonucleotide Delivery to Cells and Tissues. *Methods Mol. Biol.* **2008**, *433*, 141–158.

(195) Sperling, R. A.; Parak, W. J. Surface Modification, Functionalization and Bioconjugation of Colloidal Inorganic Nanoparticles. *Philos. Trans. R. Soc. London A Math. Phys. Eng. Sci.* **2010**, *368* (1915), 1333–1383.

(196) Nowak-Sliwinska, P.; Segura, T.; Iruela-Arispe, M. L. The Chicken Chorioallantoic Membrane Model in Biology, Medicine and Bioengineering. *Angiogenesis* **2014**, *17* (4), 779–804.

(197) Ribatti, D. Chicken Chorioallantoic Membrane Angiogenesis Model. *Methods Mol. Biol.* **2012**, *843*, 47–57.

(198) Choudhari, Y.; Reddy, U.; Monsuur, F.; Pauly, T.; Hoefer, H.; McCarthy, W. Comparative Evaluation of Porous Silica Based Carriers for Lipids and Liquid Drug Formulations. *Mesoporous Biomater.* **2014**, *1* (1).

(199) Dominska, M.; Dykxhoorn, D. M. Breaking down the Barriers: siRNA Delivery and Endosome Escape. **2010**, *123* (8), 1183–1189.

(200) Florea, B. I.; Meaney, C.; Junginger, H. E.; Borchard, G. Transfection Efficiency and Toxicity of Polyethylenimine in Differentiated Calu-3 and Nondifferentiated COS-1 Cell Cultures. *AAPS PharmSci* **2002**, *4* (3), 1–11.

(201) Kafil, V.; Omidi, Y. Cytotoxic Impacts of Linear and Branched Polyethylenimine Nanostructures in A431 Cells. *Bioimpacts* **2011**, *1* (1), 23–30.

(202) Kikuchi, S.; Tominaga, D.; Arita, M.; Takahashi, K.; Tomita, M.; Miyake, J. Dynamic Modeling of Genetic Networks Using Genetic Algorithm and S-System. *Bioinformatics* **2003**, *19* (5), 643–650.

ISBN 978-952-12-3675-4